A Distributed Feedback Motion Planning Protocol for Multiple Unicycle Agents of Different Classes

Dimitra Panagou

***Abstract*—This paper presents a novel feedback method for the motion planning and coordination of multiple agents that belong to two classes, namely class-A and class-B. All agents are modeled via unicycle kinematics. Agents of class-B do not share information with agents of class-A and do not participate in ensuring safety, modeling thus agents with failed sensing/communication systems, agents of higher priority, or moving obstacles with known upper bounded velocity. The method is built upon a family of 2-dimensional analytic vector fields, which under mild assumptions are proved to be safe feedback motion plans with a unique stable singular point. The conditions which ensure collision free and almost global convergence for a single agent and the analytical form of the vector fields are then utilized in the design the proposed distributed, semi-cooperative multi-agent coordination protocol. Semi-cooperative coordination has been defined in prior work as the ad-hoc prioritization and conflict resolution among agents *of the same class*; more specifically, participation in conflict resolution and collision avoidance for each agent is determined on-the-fly based on whether the agent's motion results in decreasing its distance with respect to its neighbor agents; based on this condition, the agent decides to either ignore its neighbors, or adjust its velocity and avoid the neighbor agent with respect to which the rate of decrease of the pairwise inter-agent distance is maximal. The proposed coordination protocol builds upon this logic and addresses the case of multiple agents *of distinct classes* (class-A and class-B) in conflict. Guarantees on the safety of the multi-agent system and the almost global convergence of the agents to their destinations are proved. The efficacy of the proposed methodology is demonstrated via simulation results in static and dynamic environments.**

I. Introduction

Motion planning, coordination and control for autonomous systems still remains an active research topic in many respects. The primary motivation is the computation of safe and efficient trajectories for robotic agents, mechanisms and autonomous vehicles which operate in constrained and/or uncertain environments. Various formulations and methodologies on the motion planning problem, ranging from Lyapunov-based methods, to sampling-based planning, to combinatorial planning, to formal methods for high-level tasking [1]–[6], have been developed within the robotics community. Multi-robot systems have attracted the interest of the control community as well, with emphasis being given to consensus, flocking and formation control problems for multiple agents, see [7] for a recent overview.

Dimitra Panagou is with the Department of Aerospace Engineering, University of Michigan, Ann Arbor, MI, USA; dpanagou@umich.edu.

The author would like to acknowledge the support of the Automotive Research Center (ARC) in accordance with Cooperative Agreement W56HZV-14-2-0001 U.S. Army TARDEC in Warren, MI, and of the NASA Grant NNX16AH81A.

Avoiding obstacles and inter-agent collisions is a requirement of highest priority in many applications. Recently, significant interest has been paid to the high-level tasking, where the problem for an autonomous agent has transitioned from the classical motion planning formulation "move from point A to point B" to the consideration of complex goals under temporal specifications such as: "visit region A, and then visit either region B or region C". Despite the significant contributions which provide elegant solutions with rigorous guarantees under certain assumptions on the considered environments [2]–[4], the interconnection of high-level tasking with the physical layer/system is still an open problem. Among the challenges towards making the link between high-level and low-level planning and control are the consideration of multiple agents in dynamic environments, and the associated complexity in finding provably correct solutions in the presence of nonlinearities, arbitrary constraints, and uncertainty.

In fact, the case of multiple agents moving safely towards goal configurations is challenging even in the absence of static obstacles and complex temporal goals. Agents typically make decisions on their actions based on information that can be locally measured using onboard sensors, or transmitted and received across the nodes of the multi-agent system via wireless communication links. In this context, consensus and formation control in multi-agent networks have been popular topics of interest, and numerous elegant solutions, which this paper cannot cite in their entirety for reasons of space, have been developed using tools and notions from graph theory, matrix theory and Lyapunov stability theory; indicatively, the interested reader is referred to [7]–[12]. Practical considerations such as anisotropic sensing of the agents have motivated the study of coordination under directed information exchange [13]–[17], while consensus for systems with nonlinear dynamics has also received significant attention [18]–[22]. Avoiding collisions in consensus, flocking, and formation control settings is typically done by selecting initial conditions carefully, and regulating relative distances and orientations to proper values.

1) Overview: This paper is motivated by problems on the motion planning for multiple agents of different classes (in terms of sensing/communication and priorities) that are assigned to reach *specific destinations*;[1] as an ultimate potential application consider the traffic management for multiple unmanned aerial systems in urban environments. We provide a novel feedback solution to the multi-agent motion planning and coordination problems in constrained dynamic environ-

[1]In that respect, the proposed problem formulation does not fall in the category of consensus, flocking or formation control problems.

ments, i.e., in environments where agents have limited sensing and communication capabilities and which are populated by moving obstacles. Two classes of agents are considered, called agents of class-A and agents of class-B. Class-A agents are assigned to safely move to specific destinations while resolving conflicts in a distributed fashion, i.e., by sharing information on their states and velocities only when they become spatially connected, see also the Assumptions 1-5 on the adopted communication protocol in Section V-A. Class-B agents do not share information with other agents and do not actively participate in ensuring safety; hence, they can model agents with failed sensing/communication and/or actuation systems, or agents of higher priority, or simply moving obstacles. Hence here we are primarily interested in designing feedback low-level controllers on the conflict resolution among multiple agents belonging to distinct classes, that can furthermore be combined with high-level tasks, such as dynamic coverage [23], or multiple tasks encoding safety and optimality [24], or even temporal tasks. The proposed planning and control is based on semi-cooperative coordination, which has been defined in our prior work [25] as the ad-hoc prioritization among agents of the *same* class. More specifically, under the coordination protocol in [25], participation in conflict resolution and collision avoidance for each agent is determined based on whether its motion results in decreasing its distance with respect to (w.r.t.) its neighbor agents; based on this condition, the agent decides to either ignore its neighbors (what we call ad-hoc prioritization), or adjust its velocity and avoid the neighbor agent w.r.t. which the rate of decrease of the pairwise inter-agent distance is maximal. This way, collision avoidance is not necessarily pursued by all agents in conflict, but rather by at least one agent in a pairwise setting, see also the Definitions 5-6 on "semi-cooperative" collision avoidance in Section V-B. Here we build upon and extend the semi-cooperative protocol in [25] to address the case multiple agents of *both class-A and class-B* in conflict. The technical tools which we use towards this goal are set-invariance methods, which have been proved efficient in constrained control problems for a class of nonlinear, underactuated systems [26].

The main ingredient of the proposed method is a family of two-dimensional analytic vector fields, originally introduced in [27], whose analytical expression is:

$$\mathbf{F}(\boldsymbol{r}) = \lambda(\boldsymbol{p}^T\boldsymbol{r})\boldsymbol{r} - \boldsymbol{p}(\boldsymbol{r}^T\boldsymbol{r}), \tag{1}$$

where $\lambda \in \mathbb{R}$ is a parameter to be specified later on, $\boldsymbol{r} = [x \;\; y]^T$ the position vector w.r.t. a global cartesian frame and $\boldsymbol{p} = [p_x \;\; p_y]^T$, with $\boldsymbol{p} \neq \mathbf{0}$.[2] The family of vector fields (1) was employed in [27], [28] for steering kinematic, drift-free systems in chained form in *obstacle-free* environments.

In this paper we first show that, except for a *known* value of the parameter λ, namely except for $\lambda = 1$, the vector field (1) has a unique singular point on $\mathbb{R}^2$ and a reflection axis. We then consider the single-agent case, i.e., a robot with unicycle kinematics in a static environment of circular obstacles and propose a blending mechanism between attractive (for $\lambda = 2$) and repulsive (for $\lambda = 1$ and $\lambda = 0$) vector fields, which under mild, explicit conditions yields almost global feedback motion plans. In other words, we define vector fields whose integral curves are by construction collision free and convergent to a goal configuration except for a set of initial conditions of Lebesgue measure zero, that is as well stated explicitly. The proposed design yields simple feedback control laws that force the system to flow along the vector field.

We finally utilize the conditions which generate almost global feedback motion plans for the single-agent case and propose a protocol for the multi-agent case involving agents of both class-A and class-B. We build upon and extend the coordination protocol introduced in [25]; more specifically, we design a protocol that forces class-A agents to resolve conflicts among each other in the semi-cooperative spirit described earlier, and furthermore ensures that collisions with class-B agents are avoided as well. The existence of Zeno trajectories for the multi-agent system that lead to possible deadlocks is studied and analyzed. The proposed method yields collision-free and almost globally convergent trajectories for the multi-agent system.

2) Relevant Earlier Work: Motion planning and collision avoidance is arguably a well-studied topic with solutions based on, among others, Lyapunov-like scalar functions, such as the avoidance functions [29], potential functions [30], [31] and navigation functions [32]–[34], harmonic functions [35], [36], stream functions [37] and vortex fields [38]. Methods based on scalar functions can provide closed-form solutions with certain guarantees [39], however they suffer from the drawback of the appearance of possible local minima away from the goal point. Navigation functions and harmonic functions overcome this limitation but under some cost: the caveat in the former case is that the Morse property which guarantees the non-existence of local minima is obtained after a parameter included in the definition of the function exceeds a lower bound, which is not a priori known. In the latter case, the computational cost of constructing harmonic functions is quite demanding. The idea of *directly* defining vector fields as feedback motion plans has been studied as well. In [40] simple smooth vector fields are locally constructed in given convex cell decompositions of polygonal environments, so that their integral curves are by construction collision-free and, in a sequential composition spirit, convergent to a goal point. The method presumes the existence of a high-level discrete motion plan which determines the successive order of the cells from an initial to a final configuration. Other relevant work employing vector fields for vehicle navigation is given in [41]–[43]. In multi-agent settings, there have been numerous elegant solutions on consensus, flocking and formation control problems [7] which address motion coordination and collision avoidance using Lyapunov-based designs, yet under certain assumptions on the agent modeling and information sharing.

3) Contributions: The main contribution of this paper w.r.t. earlier relevant work relies on the proposed motion planning and coordination protocol. More specifically: We consider two classes of agents, namely class-A and class-B, with class-B including agents that do not share information with other agents and do not participate in conflict resolution and

[2]The role the vector $\boldsymbol{p} \in \mathbb{R}^2$ plays in the properties of the vector field (1) becomes evident later on in Theorem 2.

collision avoidance. Decisions on avoiding collisions are made by class-A agents only. We propose a novel coordination (conflict resolution and collision avoidance) algorithm for class-A agents, which is distributed in the sense that agents make decisions based on information shared only locally, i.e., only when agents become spatially connected, and semi-cooperative in the sense that agents of class-A are prioritized ad-hoc once they become spatially connected, and participate in conflict resolution and collision avoidance based on whether they are about to violate safety. More specifically, agents of class-A first share information with their class-A neighbors about whether they are in conflict with class-B agents; based on this condition, class-A agents either take action to cooperatively avoid class-B agents, or they are subsequently prioritized to resolve class-A conflicts based on the maximal rate of change of their inter-agent distances. The resulting behavior of the multi-agent system is that not all agents of class-A necessarily end up in participating in collision avoidance; due to the ad-hoc prioritization, some class-A agents may decide to ignore some of their class-A agents. As a consequence, not all agents of class-A need to deviate from their original paths, yet collision avoidance is guaranteed. *To the best of our knowledge, the proposed coordination protocol, as well as the vector field-based control design are novel and have not been presented before, while the developed on-the-fly decision making and control is relevant to applications such as traffic management of unmanned aerial systems, and coordination of mobile robots in confined environments.*

In addition, other features that further differentiate our approach from similar methods are: (i) The method imposes explicit minimum clearance among agents while keeping bounded control inputs, something which typically is not the case with pure gradient-based solutions [33], [34], [44]. This characteristic is desirable from a practical viewpoint when considering multiple robots in confined environments. (ii) No parameter tuning is needed in order to render the desired convergence properties, as opposed to other methods such as [32]; the values of the parameter λ of the vector field remain fixed and are known *a priori*. (iii) Neither the computation of a cell decomposition of the free space, nor the existence of a high-level discrete motion plan are required, as opposed to [40]. (iv) The orientations of the robots can converge to any predefined values, as opposed to [41]–[43].

Remark 1: While here we consider circular obstacle environments, ongoing work reveals that the method can be also used in polygonal environments, see [45]. The case of multiple agents moving among physical obstacles of arbitrary shape under uncertainty is beyond the limits of the current paper, and is left open for future research; a relevant discussion is given in the last section.

Remark 2: It is furthermore worth noticing that the associated control design and analysis is based on set invariance concepts rather than Lyapunov-based methods. This in principle provides less conservative solutions [46] from a theoretical viewpoint, while at the same time it offers a framework which might be suitable for the consideration of complex dynamical models; a relevant example is the one studied in [26].

Compared to the author's earlier work on planning, coordination and control with vector field approaches, the problem considered here is not the same with the one in [47]. The proposed coordination protocol, as well as the accompanied technical developments, are not the same with the ones in [25] either; here the feedback plan for each agent is derived out of a vector field instead of a barrier function, and furthermore the current paper addresses the case of more than one agent of class-B in the group, while the adopted information sharing pattern differs compared to the one adopted in [25].

Part of this work has appeared in [48], [49]. The current paper additionally includes: (i) a detailed presentation of the overall method both for the static and the dynamic case, along with the proofs which have been omitted in the conference papers in the interest of space, (ii) the explicit consideration of multiple class-B agents, as well as a new motion coordination protocol that is based on different patterns of information exchange among connected agents, (iii) more simulation results which demonstrate the efficacy of the method in static and dynamic environments.

4) Organization: The paper is organized as follows: Section II includes a brief overview of the notions regarding the topology of two-dimensional vector fields that are used throughout the paper. Section III characterizes the singular points of our vector fields w.r.t. the parameter λ, while section IV presents the blending mechanism among vector fields, the construction of the almost global feedback motion plans and the underlying control design. Section V presents the extension of the method to the distributed semi-cooperative coordination of multiple agents. Our conclusions and thoughts on future work are summarized in Section VI.

II. Singular points of vector fields

This section provides an overview of notions from vector field topology. For more information the reader is referred to [50]–[52].

Definition 1: A vector field on an open subset $U \subset \mathbb{R}^n$ is a function which assigns to each point $p \in U$ a vector $X_p \in T_p(\mathbb{R}^n)$, where $T_p(\mathbb{R}^n)$ is the tangent space of $\mathbb{R}^n$ at the point p. A vector field on $\mathbb{R}^n$ is C^∞ (smooth) if its components relative to the canonical basis are C^∞ functions on U.

Definition 2: Given a C^∞ vector field X on $\mathbb{R}^n$, a curve $t \to F(t)$ defined on an open interval J of $\mathbb{R}$ is an integral curve of X if $\frac{\mathrm{d}F}{\mathrm{d}t} = X_{F(t)}$ on J.

Definition 3: A point p of U at which $X_p = 0$ is called a singular, or critical, point of the vector field.

Center-type and non-center type singularities: Singular points are typically distinguished to those that are reached by no integral curve (called *center* type) and those that are reached by at least two integral curves (called *non-center* type). In the case of a center type singularity, one can find a neighborhood of the singular point where all integral curves are closed, inside one another, and contain the singular point into their interior. In the case of non-center type singularities, one has that at least two integral curves converge to the singular point. The local structure of a non-center type singularity is analyzed by considering the behavior of all the integral curves which pass through the neighborhood of the singular point.

This neighborhood is made of several curvilinear sectors. A curvilinear sector is defined as the region bounded by a circle C of arbitrary small radius, and two integral curves, S and S', which both converge (for either $t \to +\infty$, or $t \to -\infty$) to the singular point. The integral curves passing through the open sector g (i.e., the integral curves except for S, S') determine the following three possible types of curvilinear sectors [53]: (i) *Elliptic* sectors: all integral curves begin and end at the critical point. (ii) *Parabolic* sectors: just one end of each integral curve is at the critical point. (iii) *Hyperbolic* sectors: the integral curves do not reach the critical point at all. The integral curves that separate each sector from the next are called separatrixes, see also Fig. 1.

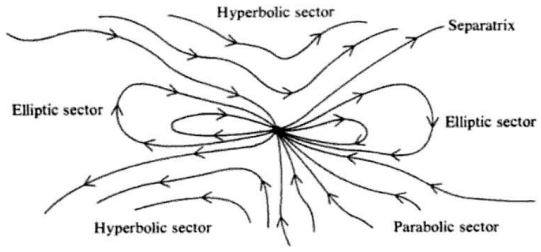

Fig. 1. A typical isolated critical point. Image taken from [51].

First-order and high-order singularities: A singular point p of a vector field X on $\mathbb{R}^2$ is called a *first-order* singular point if the Jacobian matrix $\boldsymbol{J}_X(\cdot)$ of the vector field X does not vanish (i.e., is nonsingular) on p, i.e., if: $\det(\boldsymbol{J}_X(p)) \neq 0$; otherwise the singular point is called *high-order* singular point.

III. Motion planning via vector fields

Consider the motion of a robot with unicycle kinematics in an environment $\mathcal{W}$ with N static circular obstacles. The equations of motion read:

$$\begin{bmatrix} \dot{x} \\ \dot{y} \\ \dot{\theta} \end{bmatrix} = \begin{bmatrix} \cos\theta & 0 \\ \sin\theta & 0 \\ 0 & 1 \end{bmatrix} \begin{bmatrix} u \\ \omega \end{bmatrix}, \tag{2}$$

where $\boldsymbol{q} = \begin{bmatrix} \boldsymbol{r}^T & \theta \end{bmatrix}^T$ is the configuration vector, $\boldsymbol{r} = [x \;\; y]^T$ is the position and θ is the orientation of the robot w.r.t. a global frame $\mathcal{G}$, and u, ω are the linear and the angular velocity of the robot, respectively. The robot is modeled as a closed circular disk of radius ϱ, and each obstacle $\mathcal{O}_i$ is modeled as a closed circular disk of radius ϱ_{oi} centered at $\boldsymbol{r}_{oi} = [x_{oi} \;\; y_{oi}]^T$, $i \in \{1, \ldots, N\}$. Denote $\mathcal{O}_i = \{\boldsymbol{r} \in \mathbb{R}^2 \mid \|\boldsymbol{r} - \boldsymbol{r}_{oi}\| \leq \varrho_{oi}\}$.

A. A family of vector fields for robot navigation

We consider the class of vector fields $\mathbf{F} : \mathbb{R}^2 \to \mathbb{R}^2$ given by (1). The vector field components F_x, F_y read:

$$\mathrm{F}_x = (\lambda - 1)p_x x^2 + \lambda p_y xy - p_x y^2, \tag{3a}$$
$$\mathrm{F}_y = (\lambda - 1)p_y y^2 + \lambda p_x xy - p_y x^2. \tag{3b}$$

Theorem 1: The origin $\boldsymbol{r} = \mathbf{0}$ is the unique singular point of the vector field $\mathbf{F}$ if and only if $\lambda \neq 1$.

Proof: It is straightforward to verify that $\boldsymbol{r} = \mathbf{0}$ is a singular point of $\mathbf{F}$. Let us write the vector field components (3) of $\mathbf{F}$ in matrix form as:

$$\begin{bmatrix} \mathrm{F}_x \\ \mathrm{F}_y \end{bmatrix} = \underbrace{\begin{bmatrix} (\lambda-1)x^2 - y^2 & \lambda xy \\ \lambda xy & (\lambda-1)y^2 - x^2 \end{bmatrix}}_{\boldsymbol{A}(\lambda, \boldsymbol{r})} \begin{bmatrix} p_x \\ p_y \end{bmatrix}. \tag{4}$$

The determinant of the matrix $\boldsymbol{A}(\lambda, \boldsymbol{r})$ is: $\det(\boldsymbol{A}(\lambda, \boldsymbol{r})) = -(\lambda - 1)(x^2 + y^2)^2$. This implies that $\boldsymbol{A}(\lambda, \boldsymbol{r})$ is nonsingular away from the origin $\boldsymbol{r} = \mathbf{0}$ if and only if $\lambda \neq 1$. Therefore, for $\lambda \neq 1$ and $\boldsymbol{r} \neq \mathbf{0}$, one has $\mathbf{F} = \mathbf{0}$ if and only if $\boldsymbol{p} = \mathbf{0}$. Since $\boldsymbol{p} \neq \mathbf{0}$ by definition, if follows that the vector field $\mathbf{F}$ is nonsingular everywhere but the origin $\boldsymbol{r} = \mathbf{0}$, as long as $\lambda \neq 1$. ∎

Theorem 2: The line $l : y = \tan\varphi \, x$, where $\tan\varphi \triangleq \frac{p_y}{p_x}$, is an axis of reflection, or mirror line, for $\mathbf{F}$. The proof is given in Appendix A.

Remark 3: The Jacobian matrix of $\mathbf{F}$ is singular at $\boldsymbol{r} = \mathbf{0}$, which implies that $\boldsymbol{r} = \mathbf{0}$ is a high-order singularity. Thus, one may expect that the pattern of the integral curves around the singular point is more complicated compared to those around a first-order singularity, i.e., around nodes, saddles, foci or centers [51].

Theorem 3: The equation of the integral curves of $\mathbf{F}$ for $\boldsymbol{p} = [1 \;\; 0]^T$ is given as:

$$(x^2 + y^2)^{\frac{\lambda}{2}} = c \, y^{(\lambda - 1)}, \;\; c \in \mathbb{R}. \tag{5}$$

The proof is given in Appendix B.

Remark 4: It is straightforward to verify that:

- For $\lambda = 0$, (5) reduces to $y = c$, i.e., the integral curves are straight lines parallel to $\boldsymbol{p} = [1 \;\; 0]^T$.
- For $\lambda = 1$, (5) reduces to $\sqrt{x^2 + y^2} = c$, i.e., the integral curves are circles of radius c, where $c > 0$, centered at the origin $(x, y) = (0, 0)$.

1) Attractive vector fields: Let us consider the case $\lambda = 2$. Take for simplicity $\boldsymbol{p} = [1 \;\; 0]^T$ and write the vector field components as:

$$\mathrm{F}_x = x^2 - y^2, \tag{6a}$$
$$\mathrm{F}_y = 2xy. \tag{6b}$$

Following [51], the singular point $\boldsymbol{r} = \mathbf{0}$ of (6) is a dipole; more specifically, the vector field (6) has two elliptic sectors, with the axis $y = 0$ serving as the separatrix. This implies that all integral curves *begin and end at* the singular point, *except for* the separatrix $y = 0$. The separatrix converges to $\boldsymbol{r} = \mathbf{0}$ for $x < 0$ and diverges for $x > 0$ (Fig. 2). Out of Theorem 2, the separatrix $y = 0$ is the reflection line for (6).

Furthermore, Theorem 2 implies that the axis the vector $\boldsymbol{p} \neq \mathbf{0}$ lies on is, in general, a reflection line for (1). This means that the resulting integral curves are symmetric w.r.t. the vector $\boldsymbol{p} \in \mathbb{R}^2$. In that sense, any of the integral curves of $\mathbf{F}$ offers a path to $\boldsymbol{r} = \mathbf{0}$, while at the same time the direction of the vector $\boldsymbol{p}$ dictates the symmetry axis of the integral curves w.r.t. the global frame $\mathcal{G}$.

Therefore, defining a feedback motion plan for steering the unicycle to a goal configuration $\boldsymbol{q}_g = \begin{bmatrix} \boldsymbol{r}_g^T & \theta_g \end{bmatrix}^T$ has been

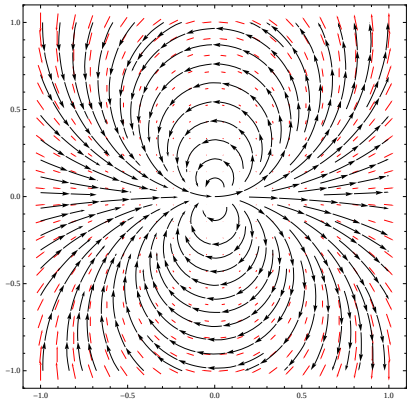

Fig. 2. The integral curves of (1) for $\lambda = 2$, $p_x = 1$, $p_y = 0$.

based in earlier work of ours' [27] on the following simple idea: Pick a vector field $\mathbf{F}$ out of (1) in terms of $(\boldsymbol{r}-\boldsymbol{r}_g)$,[3] with $\lambda = 2$ and $\boldsymbol{p} = [p_x \;\; p_y]^T$, so that the direction of the vector $\boldsymbol{p}$ coincides with the goal orientation: $\varphi \triangleq \arctan(\frac{p_y}{p_x}) = \theta_g$. Then, the integral curves serve as a reference to steer the position trajectories $\boldsymbol{r}(t)$ to the goal position $\boldsymbol{r}_g$, and the orientation trajectories $\theta(t)$ to the goal orientation θ_g.

2) Repulsive vector fields: Let us consider the case $\lambda = 1$, i.e., the case when the vector field (1) has multiple singular points. The vector field components read:

$$\mathrm{F}_x = p_y xy - p_x y^2, \tag{7a}$$
$$\mathrm{F}_y = p_x xy - p_y x^2. \tag{7b}$$

The vector field (7) vanishes on the set $\mathcal{V} = \{\boldsymbol{r} \in \mathbb{R}^2 \mid p_y x - p_x y = 0\}$. Out of Theorem 2, the singularity set $\mathcal{V}$ coincides with the reflection line of the vector field (7). The equation of the integral curves can be computed for $p_y x - p_x y \neq 0$ as: $\frac{dx}{dy} = \frac{y}{-x} \Rightarrow x^2 + y^2 = c^2$, where $c \in \mathbb{R}$, which implies that the integral curves are circles centered at $\boldsymbol{r} = \mathbf{0}$, see Fig. 3.

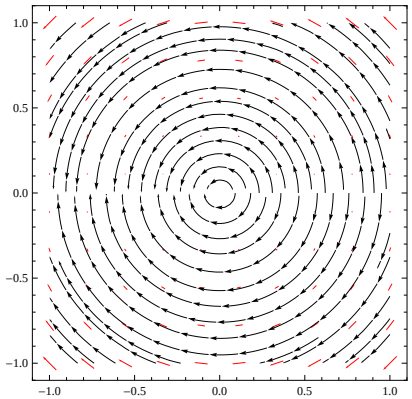

Fig. 3. The vector field $\mathbf{F}$ for $\lambda = 1$ and $p_x = 1$, $p_y = 0$.

The signum of x (in general, of ${\boldsymbol{p}_i}^T\boldsymbol{r}$) dictates whether the integral curves escape the singularity set $\mathcal{V}$ (see the half-plane $x > 0$) or converge to the singularity set $\mathcal{V}$ (see the half-plane $x < 0$). We say that the singular point $\boldsymbol{r} = \mathbf{0}$ of the vector field (7) is of center type; this means that *no integral curve reaches the singular point.*[4]

Thus, one may employ (7) to define tangential vector fields locally around circular obstacles. The definition of the repulsive vector fields around circular obstacles is given in detail in Section IV-B.

IV. Almost Global Feedback Motion Plans

Given the class of attractive and repulsive vector fields, the idea on defining an almost global feedback motion plan $\mathbf{F}^\star$ on the collision-free space $\mathcal{F}$ is to combine an attractive-to-the-goal vector field $\mathbf{F}_g$ with (local) repulsive vector fields $\mathbf{F}_{oi}$ around each obstacle $\mathcal{O}_i$, so that the integral curves of $\mathbf{F}^\star$: (i) converge to the goal $\boldsymbol{q}_g$, and (ii) point into the interior of $\mathcal{F}$ on the boundaries of the obstacles $\mathcal{O}_i$. The vector field $\mathbf{F}^\star$ can then serve as a feedback motion plan on $\mathcal{W}$.

A. Attractive vector field to the goal

Without loss of generality we assume that $\boldsymbol{q}_g = \mathbf{0}$. An attractive-to-the-goal vector field $\mathbf{F}_g$ can be taken out of (1) for $\lambda = 2$, $\boldsymbol{p}_g = [1 \;\; 0]^T$, yielding the vector field (6) (Fig. 2). To facilitate the derivations in the analysis of Lemma 1 and Theorem 4, see later on, we consider the normalized unit vector field:

$$\mathbf{F}_g^n = \begin{cases} \frac{\mathbf{F}_g}{\|\mathbf{F}_g\|}, & \text{for } \boldsymbol{r} \neq \mathbf{0}; \\ \mathbf{0}, & \text{for } \boldsymbol{r} = \mathbf{0}. \end{cases} \tag{8}$$

The components of $\mathbf{F}_g^n$ for $\boldsymbol{r} \neq \mathbf{0}$ read: $\mathrm{F}_{gx}^n = \frac{x^2-y^2}{x^2+y^2}$, $\mathrm{F}_{gy}^n = \frac{2xy}{x^2+y^2}$.

B. Repulsive vector field w.r.t. a circular obstacle

Consider an obstacle $\mathcal{O}_i$ and the region $\mathcal{Z}_i$: $\{\boldsymbol{r} \in \mathbb{R}^2 \mid \|\boldsymbol{r} - \boldsymbol{r}_{oi}\| \leq \varrho_{\mathcal{Z}i}\}$, where $\varrho_{\mathcal{Z}i} = \varrho_{oi} + \varrho + \varrho_\varepsilon$ (Fig. 4). The parameter $\varrho_\varepsilon \geq 0$ is the minimum distance that the robot is allowed to keep w.r.t. the boundary of the obstacle.

A repulsive vector field w.r.t. the point $\boldsymbol{r}_{oi}$ can be picked out of (7) for $\boldsymbol{p}_i = [p_{xi} \;\; p_{yi}]^T$, where $p_{xi} = \cos\phi_i$, $p_{yi} = \sin\phi_i$, $\phi_i = \mathrm{atan2}(-y_{oi}, -x_{oi}) + \pi$ as:

$$\mathrm{F}_{oxi} = p_{yi}(x - x_{oi})(y - y_{oi}) - p_{xi}(y - y_{oi})^2, \tag{9a}$$
$$\mathrm{F}_{oyi} = p_{xi}(x - x_{oi})(y - y_{oi}) - p_{yi}(x - x_{oi})^2. \tag{9b}$$

The vector $\boldsymbol{p}_i$ is picked such that it lies on the line connecting the center $\boldsymbol{r}_{oi}$ of the obstacle with the goal point $\boldsymbol{r}_g = \mathbf{0}$. Therefore, the singularity set of the vector field (9) lies by construction on this line, which is also the reflection axis of (9). Denote $\mathcal{A}_i = \{\boldsymbol{r} \in \mathcal{Z}_i \mid {\boldsymbol{p}_i}^T(\boldsymbol{r} - \boldsymbol{r}_{oi}) \geq 0\}$, $\mathcal{B}_i = \{\boldsymbol{r} \in \mathcal{Z}_i \mid {\boldsymbol{p}_i}^T(\boldsymbol{r} - \boldsymbol{r}_{oi}) < 0\}$, and consider the behavior of the integral curves around the singularity set $\mathcal{V}_i = \mathcal{V}_{i1} \cup \mathcal{V}_{i2}$ (Fig. 4, dotted line). The integral curves depart from the singularity set $\mathcal{V}_{i1}$ in the region $\mathcal{A}_i$ (see the red vectors around $\mathcal{V}_{i1}$ in Fig. 4), and converge to the singularity set $\mathcal{V}_{i2}$ in the region $\mathcal{B}_i$ (note that the corresponding vectors have *not* been drawn in

[3] This is to have the unique singular point of $\mathbf{F}$ coinciding with the desired position $\boldsymbol{r}_g$.

[4] Characterizing this particular singularity as of center type is slightly inconsistent with standard notation, since in this case the singular point $\boldsymbol{r} = \mathbf{0}$ is not isolated.

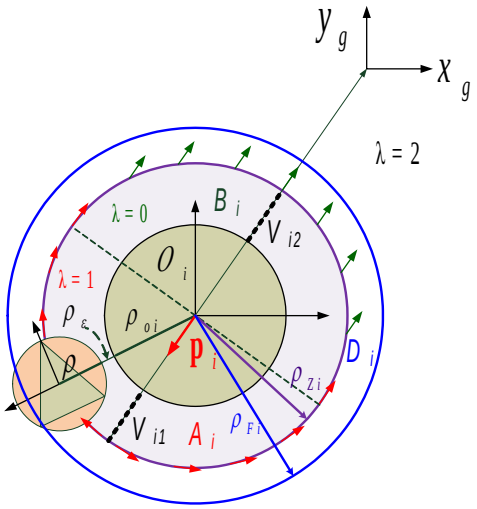

Fig. 4. Defining a repulsive vector field $\mathbf{F}_{oi}$ around the obstacle $\mathcal{O}_i$. Note that we take the vector field (1) with $\lambda = 1$ in region $\mathcal{A}_i$ and with $\lambda = 0$ in region $\mathcal{B}_i$.

Fig. 4). The integral curves in region $\mathcal{A}_i$ render safe, tangential reference paths around the obstacle $\mathcal{O}_i$. However, their pattern in region $\mathcal{B}_i$ is undesirable, since traps the system trajectories $\boldsymbol{r}(t)$ away from $\boldsymbol{r}_g$. To overcome this, in region $\mathcal{B}_i$ we define a vector field out of (1) for $\lambda = 0$ and $\boldsymbol{p}_i$ as before, (see the green vectors in Fig. 4), whose vector field components read:

$$\mathrm{F}_{oxi} = -p_{xi}(x - x_{oi})^2 - p_{xi}(y - y_{oi})^2, \tag{10a}$$
$$\mathrm{F}_{oyi} = -p_{yi}(x - x_{oi})^2 - p_{yi}(y - y_{oi})^2. \tag{10b}$$

This vector field is co-linear with $\boldsymbol{p}_i$ and vanishes at the unique singular point $\boldsymbol{r} = \boldsymbol{r}_{oi}$.

Remark 5: The transition of the integral curves between regions $\mathcal{A}_i$, $\mathcal{B}_i$ is smooth, since the vectors at the points where ${\boldsymbol{p}_i}^T(\boldsymbol{r} - \boldsymbol{r}_{oi}) = 0$ coincide.

In summary, the vector field $\mathbf{F}_{oi}$ around a circular obstacle $\mathcal{O}_i$ is picked out of the family of vector fields (1) as:

$$\mathbf{F}_{oi} = \begin{cases} \mathbf{F}_{(\lambda=1)}\left(\boldsymbol{\delta r}_i\right), & \text{if } {\boldsymbol{p}_i}^T(\boldsymbol{\delta r}_i) \geq 0; \\ \mathbf{F}_{(\lambda=0)}\left(\boldsymbol{\delta r}_i\right), & \text{if } {\boldsymbol{p}_i}^T(\boldsymbol{\delta r}_i) < 0, \end{cases} \tag{11}$$

where $\boldsymbol{\delta r}_i \triangleq \boldsymbol{r} - \boldsymbol{r}_{oi}$, $\phi_i = \operatorname{atan2}(-y_{oi}, -x_{oi}) + \pi$, $\boldsymbol{p}_i = \left[\cos\phi_i \;\; \sin\phi_i\right]^T$. Similarly to the attractive vector field case, and in order to facilitate the derivations in the analysis of Lemma 1 and Theorem 4 later on, we consider the normalized unit vector field:

$$\mathbf{F}^n_{oi} = \begin{cases} \frac{\mathbf{F}_{(\lambda=0)}(\boldsymbol{\delta r}_i)}{\|\mathbf{F}_{(\lambda=0)}(\boldsymbol{\delta r}_i)\|}, & \text{if } {\boldsymbol{p}_i}^T(\boldsymbol{\delta r}_i) < 0; \\ \frac{\mathbf{F}_{(\lambda=1)}(\boldsymbol{\delta r}_i)}{\|\mathbf{F}_{(\lambda=1)}(\boldsymbol{\delta r}_i)\|}, & \text{if } {\boldsymbol{p}_i}^T(\boldsymbol{\delta r}_i) \geq 0,\ \boldsymbol{r} \notin \mathcal{V}_i; \\ \mathbf{0}, & \text{if } {\boldsymbol{p}_i}^T(\boldsymbol{\delta r}_i) \geq 0,\ \boldsymbol{r} \in \mathcal{V}_i. \end{cases} \tag{12}$$

Remark 6: The vector fields (8) and (12) are used in the definition of the feedback motion plan $\mathbf{F}^\star$ given by (17), as described in the following Section. Note that no tuning of the parameter λ is required. In other words, the values of λ in (8), (12) are predefined (namely $\lambda = 2$ for (8), $\lambda = 0$ for the first branch in (12), and $\lambda = 1$ for the second branch in (12)), and need not to be tuned in order to obtain the desired control performance.

C. Blending attractive and repulsive vector fields

Define the obstacle function $\beta_i(\cdot) : \mathbb{R}^2 \to \mathbb{R}$ as:

$$\beta_i(\boldsymbol{r}, \boldsymbol{r}_{oi}, \varrho_{oi}) = {\varrho_{oi}}^2 - \|\boldsymbol{r} - \boldsymbol{r}_{oi}\|^2, \tag{13}$$

which is positive in the interior $\mathrm{Int}(\mathcal{O}_i)$ of the obstacle, zero on the boundary $\partial\mathcal{O}_i$ of the obstacle, and negative everywhere else. Denote the value of the constraint function β_i on the boundary $\partial\mathcal{Z}_i$ of the region $\mathcal{Z}_i$ as: $\beta_{\mathcal{Z}i} = -2\varrho_{oi}\left(\varrho + \varrho_\varepsilon\right) - \left(\varrho + \varrho_\varepsilon\right)^2$. The repulsive vector field $\mathbf{F}^n_{oi}$ is then locally defined on the set: $\left(\mathcal{Z}_i \setminus \mathrm{Int}(\mathcal{O}_i)\right) = \{\boldsymbol{r} \in \mathbb{R}^2 \mid \beta_{\mathcal{Z}i} \leq \beta_i(\boldsymbol{r}) \leq 0\}$. At the same time, the attractive vector field $\mathbf{F}^n_g$ should be defined exterior to $\mathcal{Z}_i$, i.e., for $\beta_i(\boldsymbol{r}) < \beta_{\mathcal{Z}i}$. To encode this, define the function $\sigma_i(\cdot) : \mathbb{R}^2 \to [0, 1]$:

$$\sigma_i = \begin{cases} 1, & \text{for } \beta_i(\boldsymbol{r}) < \beta_{\mathcal{F}i}; \\ a{\beta_i}^3 + b{\beta_i}^2 + c\beta_i + d, & \text{for } \beta_{\mathcal{F}i} \leq \beta_i(\boldsymbol{r}) \leq \beta_{\mathcal{Z}i}; \\ 0, & \text{for } \beta_{\mathcal{Z}i} < \beta_i(\boldsymbol{r}); \end{cases} \tag{14}$$

where $\beta_{\mathcal{Z}i}$ is the value of (13) at distance $\varrho_{\mathcal{Z}i}$ w.r.t. $\boldsymbol{r}_{oi}$, $\beta_{\mathcal{F}i}$ is the value of (13) at some distance $\varrho_{\mathcal{F}i} > \varrho_{\mathcal{Z}i}$ w.r.t. $\boldsymbol{r}_{oi}$. The coefficients a, b, c and d of the polynomial are computed so that the derivative of the polynomial w.r.t. β_i evaluated at the endpoints of the interval $[\beta_{\mathcal{F}i}, \beta_{\mathcal{Z}i}]$ is zero; this way the function (14) is everywhere continuously differentiable. The coefficients a, b, c and d are therefore given as the solution of the linear system:

$$\begin{bmatrix} {\beta_{\mathcal{F}i}}^3 & {\beta_{\mathcal{F}i}}^2 & \beta_{\mathcal{F}i} & 1 \\ 3{\beta_{\mathcal{F}i}}^3 & 2\beta_{\mathcal{F}i} & 1 & 0 \\ {\beta_{\mathcal{Z}i}}^3 & {\beta_{\mathcal{Z}i}}^2 & \beta_{\mathcal{Z}i} & 1 \\ 3{\beta_{\mathcal{Z}i}}^2 & 2\beta_{\mathcal{Z}i} & 1 & 0 \end{bmatrix} \begin{bmatrix} a \\ b \\ c \\ d \end{bmatrix} = \begin{bmatrix} 1 \\ 0 \\ 0 \\ 0 \end{bmatrix},$$

which yields: $a = \frac{2}{(\beta_{\mathcal{Z}i} - \beta_{\mathcal{F}i})^3}$, $b = -\frac{3(\beta_{\mathcal{Z}i} + \beta_{\mathcal{F}i})}{(\beta_{\mathcal{Z}i} - \beta_{\mathcal{F}i})^3}$, $c = \frac{6\beta_{\mathcal{Z}i}\beta_{\mathcal{F}i}}{(\beta_{\mathcal{Z}i} - \beta_{\mathcal{F}i})^3}$, $d = \frac{{\beta_{\mathcal{Z}i}}^2(\beta_{\mathcal{Z}i} - 3\beta_{\mathcal{F}i})}{(\beta_{\mathcal{Z}i} - \beta_{\mathcal{F}i})^3}$.

Having this at hand, and inspired by [40], one may now define the vector field:

$$\mathbf{F}_i = \sigma_i \mathbf{F}^n_g + (1 - \sigma_i)\mathbf{F}^n_{oi}. \tag{15}$$

Lemma 1: The vector field (15) is:

- (*i*) Attractive to the goal $\boldsymbol{q}_g$ for $\|\boldsymbol{r} - \boldsymbol{r}_{oi}\| \geq \varrho_{\mathcal{F}i}$, i.e., for $\beta_i(\boldsymbol{r}) \leq \beta_{\mathcal{F}i}$ where $\sigma_i = 1$, via the effect of $\mathbf{F}^n_g$.
- (*ii*) Repulsive w.r.t. $\mathcal{O}_i$ for $\varrho_{oi} \leq \|\boldsymbol{r} - \boldsymbol{r}_{oi}\| \leq \varrho_{\mathcal{Z}i}$, i.e., for $\beta_{\mathcal{Z}i} \leq \beta_i(\boldsymbol{r})$ where $\sigma_i = 0$, via the effect of $\mathbf{F}^n_{oi}$.
- (*iii*) Nonsingular in the region $\varrho_{\mathcal{Z}i} < \|\boldsymbol{r} - \boldsymbol{r}_{oi}\| < \varrho_{\mathcal{F}i}$, i.e., for $\beta_{\mathcal{F}i} < \beta_i(\boldsymbol{r}) < \beta_{\mathcal{Z}i}$ where $0 < \sigma_i < 1$.
- (*iv*) Safe w.r.t. the obstacle $\mathcal{O}_i$ and convergent to the goal $\boldsymbol{q}_g$ for almost all initial conditions.

The proof is given in Appendix C.

D. Motion plan in static obstacle environments

Theorem 4: Assume a workspace $\mathcal{W}$ of N circular obstacles $\mathcal{O}_i$, $i \in \{1, \ldots, N\}$, positioned such that the inter-obstacle distances $d_{ij} = \|\boldsymbol{r}_{oi} - \boldsymbol{r}_{oj}\|$ satisfy:

$$d_{ij} \geq \varrho_{\mathcal{Z}i} + \varrho_{\mathcal{Z}j},\ \forall(i, j),\ j \in \{1, \ldots, N\},\ j \neq i. \tag{16}$$

Then, the vector field $\mathbf{F}^\star : \mathbb{R}^2 \to \mathbb{R}^2$, given as:

$$\mathbf{F}^\star = \prod_{i=1}^{N} \sigma_i \mathbf{F}_g + \sum_{i=1}^{N} (1-\sigma_i)\mathbf{F}_{oi}, \tag{17}$$

where $\mathbf{F}_g$ is the normalized attractive vector field (8), $\mathbf{F}_{oi}$ is the normalized repulsive vector field (12) around an obstacle $\mathcal{O}_i$, and σ_i is the bump function (14) defined in terms of the obstacle function β_i given by (13), is a safe, almost global feedback motion plan in $\mathcal{F}$, except for a set of initial conditions of measure zero.

Proof: By construction, the first term in (17) cancels the effect of the attractive vector field $\mathbf{F}_g$ where at least one of the bump functions $\sigma_i = 0$, i.e., in the corresponding region $\mathcal{Z}_i$ around obstacle $\mathcal{O}_i$. At the same time the second term shapes the corresponding vector field $\mathbf{F}_{oi}$ in $\mathcal{Z}_i$. Thus, the attractive vector field $\mathbf{F}_g$ is activated through (17) only when $\beta_i < \beta_{\mathcal{Z}i}$ $\forall i \in \{1, \ldots, N\}$, i.e., outside the regions $\mathcal{Z}_i$. Furthermore, setting the inter-obstacle distance $d_{ij} \geq \varrho_{\mathcal{Z}i} + \varrho_{\mathcal{Z}j}$ implies that the repulsive flows around obstacles do not overlap, and therefore are both safe and almost globally convergent to the goal, as proved in Lemma 1. This completes the proof. ■

Remark 7: The condition (16) reads that the minimum distance among the boundaries of the obstacles should be at least $2(\varrho+\varrho_\varepsilon)$. This clearance is not conservative or restrictive in practice, since the parameter ϱ_ε can be chosen arbitrarily close to zero, or even equal to zero, in case the robot is allowed to touch the obstacle.

E. Control design and simulation results

Having (17) at hand, the control design for the unicycle (2) is now straightforward. We use the control law:

$$u = k_u \tanh\left(\|\boldsymbol{r} - \boldsymbol{r}_g\|\right), \tag{18a}$$

$$\omega = -k_\omega(\theta - \varphi) + \dot{\varphi}, \tag{18b}$$

where $\varphi \triangleq \arctan\left(\frac{\mathrm{F}_y^\star}{\mathrm{F}_x^\star}\right)$ is the orientation of the vector field $\mathbf{F}^\star$ at a point (x, y), with its time derivative reading:

$$\dot{\varphi} \overset{(2)}{=} \left(\left(\frac{\partial \mathrm{F}_y^\star}{\partial x}\, c\theta + \frac{\partial \mathrm{F}_y^\star}{\partial y}\, s\theta\right)\mathrm{F}_x^\star - \left(\frac{\partial \mathrm{F}_x^\star}{\partial x}\, c\theta + \frac{\partial \mathrm{F}_x^\star}{\partial y}\, s\theta\right)\mathrm{F}_y^\star\right) u,$$

where $c(\cdot) = \cos(\cdot)$, $s(\cdot) = \sin(\cdot)$, the linear velocity u given by (18a), and $k_\omega > 0$, $k_u > 0$. Then, the orientation $\theta(t)$ is Globally Exponentially Stable (GES) to the safe orientation $\varphi(t)$ and the robot flows along the integral curves of $\mathbf{F}^\star$ until converging to $\boldsymbol{r}_g$.

To demonstrate the efficacy of the proposed planning and control design we consider the motion of a robot in an environment with $N = 10$ static obstacles (Fig. 5), where the goal position is $\boldsymbol{r}_g = [-0.1 \;\; 0.08]^T$. The radii of the obstacles are set equal to $\varrho_{oi} = 0.03$. The blending zone $\mathcal{D}_i$ around each obstacle $\mathcal{O}_i$ is illustrated between the boundary surfaces S_i (black line) and T_i (red line), respectively. The resulting collision-free path under the control law (18), with the control gains picked equal to $k_u = 0.075$, $k_\omega = 2.5$, is depicted in blue color.

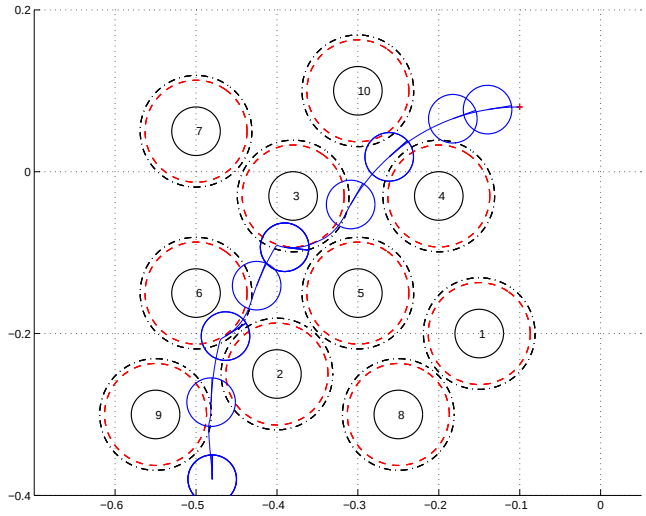

Fig. 5. The path of a unicycle in an obstacle environment.

V. Distributed Semi-Cooperative Coordination

A. Class-A and Class-B Agents

Let us now consider N identical agents $i \in \{1, \ldots, N\}$, called thereafter agents of class-A, which are assigned to move to goal locations $\boldsymbol{r}_{gi}$ while avoiding collisions. Each class-A agent i has a circular communication/sensing region $\mathcal{C}_i$ of radius R_c centered at $\boldsymbol{r}_i = \begin{bmatrix} x_i & y_i \end{bmatrix}^T$, denoted as $\mathcal{C}_i : \{\boldsymbol{r} \in \mathbb{R}^2 \mid \|\boldsymbol{r}_i - \boldsymbol{r}\| \leq R_c\}$.

Assumption 1: Each class-A agent i can sense, i.e., measure the position and orientation of any other agent (either of class-A, or of class-B, see later on) lying in $\mathcal{C}_i$.

Assumption 2: Each class-A agent i can exchange information on linear velocities with any other class-A agent $k \neq i$ lying in $\mathcal{C}_i$.

Consider also M dynamic obstacles $o \in \{N+1, \ldots, N+M\}$, i.e., objects which are moving with upper bounded linear velocity $u_o > 0$ towards arbitrary directions. These can model either agents of higher priority to the class-A agents, or adversarial agents which are non-cooperative to the motion of the class-A agents, or failed class-A agents whose motion is uncontrollable. In the sequel we refer to this class of dynamic obstacles as class-B agents.

Assumption 3: Each class-B agent o is of circular shape. Its radius r_o and the upper bounded velocity u_o is known to any class-A agent i.

Assumption 4: A class-B agent o neither receives, nor transmits, any information to a class-A agent i.

Denote $\mathcal{N}_{i,A}$ the set of class-A neighbor agents $k \neq i$ of agent i, $\mathcal{N}_{i,B}$ the set of class-B neighbor agents o of agent i, and $\mathcal{N}_i = \mathcal{N}_{i,A} \bigcup \mathcal{N}_{i,B}$ the set of neighbor agents to agent i. Safety for a class-A agent i is reduced into finding a feedback motion plan $\mathbf{F}_i^\star$ so that its integral curves point into the interior of the collision-free space $\mathcal{F}_i$ on the boundaries of the neighbor (class-A and class-B) agents, and converge to the assigned goal location $\boldsymbol{r}_{gi}$. Towards this end, we would like to employ

a vector field $\mathbf{F}_i^\star$ for each agent i as:

$$\mathbf{F}_i^\star = \prod_{j\in\mathcal{N}_i}(1-\sigma_{ij})\mathbf{F}_{gi} + \sum_{j\in\mathcal{N}_i}\sigma_{ij}\mathbf{F}_{oj}^i, \tag{19}$$

where the attractive term $\mathbf{F}_{gi}$ is taken out of (8), the repulsive term $\mathbf{F}_{oj}^i$ around each neighbor agent $j\in\mathcal{N}_i$ is defined as a normalized repelling node, given out of:

$$\mathrm{F}_{xoj}^i = \frac{x_i - x_j}{\sqrt{(x_i-x_j)^2+(y_i-y_j)^2}}, \tag{20a}$$

$$\mathrm{F}_{yoj}^i = \frac{y_i - y_j}{\sqrt{(x_i-x_j)^2+(y_i-y_j)^2}}, \tag{20b}$$

and the bump function σ_{ij} is defined as:

$$\sigma_{ij} = \begin{cases} 1, & \text{for } d_m \le d_{ij} < d_r; \\ a\ {d_{ij}}^3 + b\ {d_{ij}}^2 + c\ d_{ij} + d, & \text{for } d_r \le d_{ij} \le d_c; \\ 0, & \text{for } d_{ij} > d_c; \end{cases} \tag{21}$$

where d_{ij} is the Euclidean distance between agents i and j, $d_m \ge 2(2\varrho+\varrho_\epsilon)$ is the minimum allowable pairwise distance, d_c is a positive constant such that $d_c \le R_c$, and d_r is a positive constant such that $d_m < d_r < d_c$. The coefficients a, b, c, d have been computed similarly as the coefficients of (14) as: $a = -\frac{2}{(d_r-d_c)^3}$, $b = \frac{3(d_r+d_c)}{(d_r-d_c)^3}$, $c = -\frac{6\ d_r d_c}{(d_r-d_c)^3}$, $d = \frac{{d_c}^2(3d_r-d_c)}{(d_r-d_c)^3}$, so that (21) is a $\mathcal{C}^1$ function.

Assumption 5: Each class-A agent i transmits information to all class-A neighbors $k\in\mathcal{N}_{i,A}$ regarding to whether its set of class-B neighbors $\mathcal{N}_{i,B}$ is empty or not. In other words, each class-A agent i informs all of its class-A neighbors k on whether it is currently in conflict with at least one class-B agent o. Similarly, each class-A i receives information from its class-A neighbors on whether they are in conflict with some class-B agent or not.

This information exchange pattern is modeled via a local binary variable $\mu_i\in\{0,1\}$ for each class-A agent i according to this logic:

1) If agent i gets informed that none of its class-A neighbors is in conflict with a class-B agent, then $\mu_i = 0$.
2) If agent i gets informed that at least one of its class-A neighbors is in conflict with at least one class-B agent, then $\mu_i = 1$.

Remark 8: The set of Assumptions 1-5 describes the adopted information exchange and communication protocol. We are now ready to propose the semi-cooperative coordination protocol for the multi-agent system.

B. Coordination Protocol

To illustrate the notion of semi-cooperative coordination let us consider the following definitions [25]. Consider the time derivative of the pairwise collision avoidance constraint: $c_{ij} = (x_i-x_j)^2+(y_i-y_j)^2-{d_m}^2 \ge 0$, evaluated along the closed-loop trajectories for agent i and j, respectively, which reads:

$$\frac{d}{dt}\ c_{ij} = \underbrace{2u_i\ \boldsymbol{r}_{ji}{}^T\begin{bmatrix}\cos\theta_i\\ \sin\theta_i\end{bmatrix}}_{I}\ \underbrace{-2u_j\ \boldsymbol{r}_{ji}{}^T\begin{bmatrix}\cos\theta_j\\ \sin\theta_j\end{bmatrix}}_{J}, \tag{22}$$

where $\boldsymbol{r}_{ji} \triangleq \boldsymbol{r}_i - \boldsymbol{r}_j$ and the velocities u_i, u_j are positive by construction (this is justified later on). Denote $\boldsymbol{\eta}_i \triangleq \begin{bmatrix}\cos\theta_i & \sin\theta_i\end{bmatrix}^T$, $\boldsymbol{\eta}_j \triangleq \begin{bmatrix}\cos\theta_j & \sin\theta_j\end{bmatrix}^T$.

Definition 4: Assume that $\boldsymbol{r}_{ji}{}^T\boldsymbol{\eta}_i \ge 0$ and $\boldsymbol{r}_{ji}{}^T\boldsymbol{\eta}_j \le 0$: Then $I\ge 0$ and $J\ge 0$, which implies that both agents i, j contribute in satisfying the collision avoidance condition. We say that collision avoidance is *"fully cooperative."*

Definition 5: Assume that $\boldsymbol{r}_{ji}{}^T\boldsymbol{\eta}_i \ge 0$ and $\boldsymbol{r}_{ji}{}^T\boldsymbol{\eta}_j > 0$: Then $I\ge 0$ and $J<0$, which implies that agent i contributes towards avoiding collision, whereas agent j does not. If $I+J\ge 0$, we say that collision avoidance is *"semi-cooperative by agent i"*; otherwise, *"collision"* occurs.

Definition 6: Assume that $\boldsymbol{r}_{ji}{}^T\boldsymbol{\eta}_i < 0$ and $\boldsymbol{r}_{ji}{}^T\boldsymbol{\eta}_j \le 0$: Then $I<0$ and $J\ge 0$, which implies that agent j contributes towards avoiding collision, whereas agent i does not. If $I+J\ge 0$, we say that collision avoidance is *"semi-cooperative by agent j"*; otherwise, *"collision"* occurs.

Definition 7: Assume that $\boldsymbol{r}_{ji}{}^T\boldsymbol{\eta}_i < 0$ and $\boldsymbol{r}_{ji}{}^T\boldsymbol{\eta}_j > 0$: Then $I<0$ and $J<0$, which implies that *"collision"* occurs.

The above definitions demonstrate that there are cases when collision avoidance can be accomplished by one agent only, hence the characterization "semi-cooperative". We use this observation to build and study the correctness of the following coordination protocol.

Coordination of linear velocities: The linear velocity u_i of each agent i is governed by the control laws:

□ If $\mathcal{N}_{i,B} = \emptyset$, and $\mu_i = 0$, then:

$$u_i = \begin{cases} \max\left\{0, \min\limits_{k\in\mathcal{N}_{i,A}|J_k<0} u_{i|k}\right\}, & d_m \le d_{ik} \le d_\epsilon, \\ u_{i\epsilon}, & d_\epsilon < d_{ik} < d_c, \\ u_{ic}, & d_c \le d_{ik}; \end{cases}, \tag{23a}$$

□ If $\mathcal{N}_{i,B} \ne \emptyset$, and $\mu_i = 0$, then:

$$u_i = \begin{cases} \min\limits_{o\in\mathcal{N}_{i,B}} u_{i|o}, & d_m \le d_{io} \le d_c, \\ u_{i\epsilon}, & d_\epsilon < d_{ik} < d_c, \\ u_{ic}, & d_c < d_{io}; \end{cases}, \tag{23b}$$

□ If $\mathcal{N}_{i,B} = \emptyset$, and $\mu_i = 1$, then:

$$u_i = \begin{cases} \min\limits_{k\in\mathcal{N}_{i,A}} u_{i|k}, & d_m \le d_{ik} \le d_c, \\ u_{i\epsilon}, & d_\epsilon < d_{ik} < d_c, \\ u_{ic}, & d_c < d_{ik}; \end{cases}, \tag{23c}$$

□ If $\mathcal{N}_{i,B} \ne \emptyset$, and $\mu_i = 1$, then:

$$u_i = \begin{cases} \min\limits_{k\in\mathcal{N}_{i,A}\bigcup\mathcal{N}_{i,B}} u_{i|k}, & d_m \le d_{ik} \le d_c, \\ u_{i\epsilon}, & d_\epsilon < d_{ik} < d_c, \\ u_{ic}, & d_c < d_{ik}; \end{cases}, \tag{23d}$$

where:

- $u_{ic} = k_{ui}\tanh(\|\boldsymbol{r}_i - \boldsymbol{r}_{gi}\|)$, $k_{ui}>0$,
- $u_{i\epsilon}$ is the value of the linear velocity u_i of the agent i when $d_{ij} = d_c$, that is, $u_{i\epsilon} = u_{ic}|_{d_{ij}=d_c}$,
- the distance d_ϵ is set equal to $d_\epsilon = d_r - \epsilon$,
- $u_{i|k}$ is the safe velocity of agent i w.r.t. a class-A neighbor agent $k\in\mathcal{N}_{i,A}$, given as:

$$u_{i|k} = u_{i\epsilon}\ \frac{d_{ik}-d_m}{d_\epsilon - d_m} + \varepsilon_i\ u_{is|k}\ \frac{d_\epsilon - d_{ik}}{d_\epsilon - d_m}, \tag{24}$$

with the terms in (24) defined as:

$$u_{is|k} = u_k \frac{\boldsymbol{r}_{ki}{}^T \boldsymbol{\eta}_k}{\boldsymbol{r}_{ki}{}^T \boldsymbol{\eta}_i}, \quad \boldsymbol{\eta}_i = \begin{bmatrix} \cos\varphi_i \\ \sin\varphi_i \end{bmatrix}, \quad J_k = \boldsymbol{r}_{ki}{}^T \boldsymbol{\eta}_i,$$
$$\boldsymbol{r}_{ki} = \boldsymbol{r}_i - \boldsymbol{r}_k, \quad \text{and} \quad 0 < \varepsilon_i < 1.$$

– $u_{i|o}$ is the safe velocity of agent i w.r.t. a class-B neighbor agent $o \in \mathcal{N}_{i,B}$, given as:

$$u_{i|o} = u_{ic} \frac{d_{io} - d_m}{d_c - d_m} + u_{is|o} \frac{d_c - d_{io}}{d_c - d_m}, \quad (25)$$
$$\text{with: } u_{is|o} = \frac{u_o d_c}{\boldsymbol{r}_{io}{}^T \boldsymbol{\eta}_i}.$$

Coordination of angular velocities: The angular velocity ω_i of each agent i is governed by the control law:

$$\omega_i = -k_{\omega i} (\theta_i - \varphi_i) + \dot{\varphi}_i, \quad (26)$$

where $\varphi_i \triangleq \arctan\left(\frac{\mathrm{F}^\star_{iy}}{\mathrm{F}^\star_{ix}}\right)$ is the orientation of the vector field $\mathbf{F}^\star_i$ given by (19) at a point (x, y), and $k_{\omega i} > 0$.

Theorem 5: Consider N class-A agents $i \in \{1, \ldots, N\}$ assigned to move to goal locations $\boldsymbol{r}_{gi}$, and M class-B agents $o \in \{N+1, \ldots, N+M\}$ serving as dynamic obstacles moving with known upper bounded velocities $u_o > 0$ towards arbitrary directions. Then, under the coordination protocol (23), (26), each class-A agent safely converges to its goal configuration almost globally, except for a set of initial conditions of measure zero.

Proof: Under (26) the closed loop orientation trajectories of each class-A agent i are forced to globally exponentially track the vector field (19). If $d_{ij}(t) > d_c$, $\forall t \geq 0$ and $\forall j \in \{1, \ldots, N, N+1, \ldots, N+M\}$, then one has $\sigma_{ij}(t) = 1$, implying that agent i flows safely under (18a) along (8) and converges to $\boldsymbol{r}_{gi}$.

Let us now assume that at some time $t \geq 0$ the distance $d_{ij}(t)$ between a pair of agents (i, j) is $d_{ij}(t) \leq R_c$. Collision-free motion is realized as ensuring that $d_{ij}(t) \geq 2\varrho$, $\forall t \geq 0$, for any pair (i, j). Consider the time derivative of the inter-agent distance function, which after some calculations reads:

$$\frac{d}{dt} d_{ij} \overset{(2)}{=} \frac{u_i \, \boldsymbol{r}_{ji}{}^T \boldsymbol{\eta}_i - u_j \, \boldsymbol{r}_{ji}{}^T \boldsymbol{\eta}_j}{d_{ij}}. \quad (27)$$

The analysis on the safety and technical correctness of the proposed velocity coordination protocol (23) is presented in the four following Lemmas.

Lemma 2: Assume that agent i has class-A neighbors $j \in \mathcal{N}_{i,A}$ only, i.e., $\mathcal{N}_{i,B} = \emptyset$, and also that none of the agents j is in conflict with a class-B agent, i.e., $\mu_i = 0$. Then under (23a), agent i avoids collision with any of its neighbors $j \in \mathcal{N}_i$.

Proof: Under the control law (23a), agent i adjusts its linear velocity u_i according to the velocity profile shown in Fig. 6, given analytically out of (24), so that the distance d_{ij} w.r.t. the worst case neighbor j remains greater than d_m. The worst case neighbor is defined as the agent $j \in \{\mathcal{N}_{i,A} | J_j < 0\}$ towards whom the rate of change of relative distance d_{ij} given by (27), due to the motion of agent i, is maximum. More specifically: The term $J_j < 0$ describes the set of neighbor agents j of agent i towards whom agent i is moving [25].

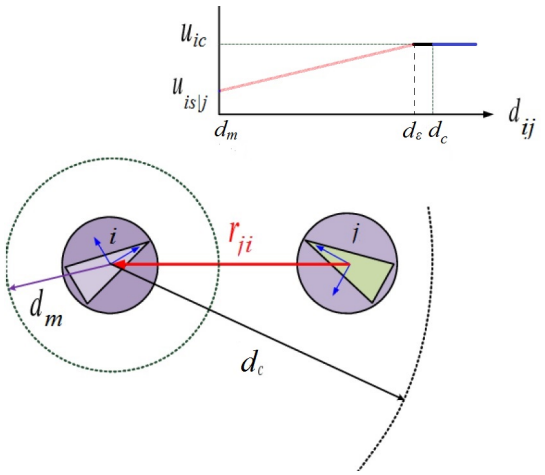

Fig. 6. If $J_j \triangleq \boldsymbol{r}_{ji}{}^T \boldsymbol{\eta}_i < 0$, i.e., if agent i moves towards agent j, then agent i adjusts its linear velocity according to the velocity profile shown here, given analytically by (24).

Thus agent i computes safe velocities $u_{i|j}$ w.r.t. each neighbor $j \in \{\mathcal{N}_{i,A} | J_j < 0\}$, and picks the minimum $\min u_{i|j}$ of the safe velocities so that the first term in (27) is as less negative as possible. Now, the value of the safe velocity $u_{i|j}$ (24) when $d_{ij} = d_m$ is by construction equal to $\varepsilon_i u_{is|k} = \varepsilon_i u_j \frac{\boldsymbol{r}_{ji}{}^T \boldsymbol{\eta}_j}{\boldsymbol{r}_{ji}{}^T \boldsymbol{\eta}_i}$. Plugging this value into (27) reads:

$$\frac{d}{dt} d_{ij} = \frac{(\varepsilon_i - 1) u_j \, \boldsymbol{r}_{ji}{}^T \boldsymbol{\eta}_j}{d_{ij}} \geq 0.$$

To see why this condition is true, recall that $\varepsilon_i - 1 < 0$, $u_j \geq 0$, and $\boldsymbol{r}_{ji}{}^T \boldsymbol{\eta}_j \leq 0$: this is because agent j is either following a vector field $\mathbf{F}^\star_j$ that points away from agent i, or happens to move away from agent i in the first place. This implies that the inter-agent distance d_{ij} can not become less than d_m. Since by definition $d_m > 2\varrho$, this further implies that collisions are avoided.

Finally, if the minimum safe velocity $\min u_{i|j}$ is negative, then (23a) forces agent i to obtain zero linear velocity (stop moving); this is in order to prevent back-to-back collisions between pairs of class-A agents (i, j) who get to move backwards under $\min u_{i|j}$ in order to avoid their class-A neighbors, *yet they do not consider each other in their individual selections of neighbors-to-avoid because the conditions $J_j < 0$, $J_i < 0$ are not met for their relative configurations.* ■

Lemma 3: Assume that agent i has at least one class-B neighbor o, i.e., $\mathcal{N}_{i,B} \neq \emptyset$, and also that none of its class-A neighbors $k \in \mathcal{N}_{i,A}$ is in conflict with a class-B agent, i.e., $\mu_i = 0$. Then under (23b), agent i avoids (i) all its class-B neighbors $o \in \mathcal{N}_{i,B}$ and (ii) all its class-A neighbors $k \in \mathcal{N}_{i,A}$.

Proof: This case is same in spirit with the case above, with the difference that agent i now considers its class-B neighbors $o \in \mathcal{N}_{i,B}$ only. The control law (23b) forces agent i to adjust its linear velocity u_i so that it avoids the class-B neighbor $o \in \mathcal{N}_{i,B}$ whose motion maximizes the rate of change of relative distance d_{io}. The avoidance of class-A neighbors $k \in \mathcal{N}_{i,A}$ is ensured indirectly via the motion of the class-A neighbors k under (23c), see the case later on. ■

Lemma 4: Assume that agent i does not have class-B neighbors, i.e., $\mathcal{N}_{i,B} = \emptyset$, but at least one of the class-A neighbors $j \in \mathcal{N}_{i,A}$ is in conflict with a class-B agent, i.e., $\mu_i = 1$. Then under (23c), agent i avoids collision with any of its neighbors $j \in \mathcal{N}_i$.

Proof: Agent i has class-A neighbors $j \in \mathcal{N}_{i,A}$ only. Since at least one these neighbors j is in conflict with a class-B agent o, it may happen that agent j is forced under (23b) to move with negative linear velocity u_j. Thus under (23c), agent i adjusts its current linear velocity u_i to the minimum safe velocity $u_{i|j}$ w.r.t. all class-A neighbor agents $j \in \mathcal{N}_{i,A}$. Note that Lemma 4 completes also the analysis of case (ii) in Lemma 3: Namely, Lemma 4 implies that a class-A agent j (denoted i in Lemma 3) who is in conflict with a class-B neighbor o is avoided by its neighbor class-A agents $i \in \mathcal{N}_{j,A}$ (denoted $k \in \mathcal{N}_{i,A}$ in Lemma 3). ■

Lemma 5: Assume that agent i has class-B neighbors, i.e., $\mathcal{N}_{i,B} \neq \emptyset$, and at least one of the class-A neighbors $j \in \mathcal{N}_{i,A}$ is in conflict with at least one class-B agent, i.e., $\mu_i = 1$. Then under (23d) agent i avoids collision with any of its neighbors $j \in \mathcal{N}_i$.

Proof: Similarly to the previous cases, agent i computes safe velocities $u_{i|j}$ w.r.t. all its neighbor agents, both class-B and class-A, and adjusts its current linear velocity u_i to the minimum out of $u_{i|j}$. ■

In order to draw conclusions about the convergence of the agents' trajectories to their goal configurations, i.e., to identify any possible deadlock situations preventing agents from converging to their assigned goal locations, we need to examine the behavior of the integral curves of the vector fields $\mathbf{F}_i^\star$, $\mathbf{F}_j^\star$ around the surfaces:

$$S_{ij}(t) : \{\boldsymbol{r}_i(t), \boldsymbol{r}_j(t) \in \mathbb{R}^2 \mid \|\boldsymbol{r}_i(t) - \boldsymbol{r}_j(t)\|^2 - {d_c}^2 = 0\},$$
$$T_{ij}(t) : \{\boldsymbol{r}_i(t), \boldsymbol{r}_j(t) \in \mathbb{R}^2 \mid \|\boldsymbol{r}_i(t) - \boldsymbol{r}_j(t)\|^2 - {d_r}^2 = 0\},$$

for any pair of agents (i, j). We focus on these surfaces since if the trajectories $\boldsymbol{r}_i(t)$, $\boldsymbol{r}_j(t)$ never cross the surfaces $S_{ij}(t)$, $\forall (i, j)$, then, as explained earlier, each one of the agents i, j moves under an attractive vector field to its goal location. Crossing the surfaces $S_{ij}(t)$ implies that the vector fields $\mathbf{F}_i^\star$, $\mathbf{F}_j^\star$ are shaped under the effect of both attractive and repulsive fields; hence, we are interested in identifying conditions under which the system trajectories $\boldsymbol{r}_i(t)$, $\boldsymbol{r}_j(t)$ are forced to get stuck (chatter) on either $S_{ij}(t)$ or $T_{ij}(t)$, *for infinite amount of time*. This can be seen as identifying sufficient conditions of the appearance of (chattering) Zeno behavior, or Zeno points [54]. A sufficient condition on the appearance of Zeno points is given in [55], Theorem 2. Based on this result, we study under which conditions the system (i.e., agents') trajectories converge to a Zeno point.

Consider the case with $N = 2$ agents. Denote the dynamics of the k-th agent as $\dot{\boldsymbol{q}}_k = \boldsymbol{f}_k(\boldsymbol{q}_k)$, $k \in \{i, j\}$, $\boldsymbol{q} = \begin{bmatrix} {\boldsymbol{q}_i}^T & {\boldsymbol{q}_j}^T \end{bmatrix}^T$, $\boldsymbol{r} = \begin{bmatrix} {\boldsymbol{r}_i}^T & {\boldsymbol{r}_j}^T \end{bmatrix}^T$, and take:

$$\nabla S_{ij} \boldsymbol{f}(\boldsymbol{q}) = 2u_i \, {\boldsymbol{r}_{ij}}^T \begin{bmatrix} \cos\theta_i \\ \sin\theta_i \end{bmatrix} - 2u_j \, {\boldsymbol{r}_{ij}}^T \begin{bmatrix} \cos\theta_j \\ \sin\theta_j \end{bmatrix}, \quad (28a)$$

$$\nabla T_{ij} \boldsymbol{f}(\boldsymbol{q}) = 2u_i \, {\boldsymbol{r}_{ij}}^T \begin{bmatrix} \cos\theta_i \\ \sin\theta_i \end{bmatrix} - 2u_j \, {\boldsymbol{r}_{ij}}^T \begin{bmatrix} \cos\theta_j \\ \sin\theta_j \end{bmatrix}, \quad (28b)$$

where $\boldsymbol{r}_{ij} = \boldsymbol{r}_i - \boldsymbol{r}_j$. Since the control law (26) renders the orientation θ_k of the k-th agent GES to the orientation φ_k of the vector field $\mathbf{F}_k^\star$, one has that the unit vector $[\cos\theta_k \quad \sin\theta_k]^T$, $k \in \{i, j\}$, in (28) coincides with the vector field $\mathbf{F}_k^\star(\boldsymbol{r}_k)$, evaluated at $\boldsymbol{r}_k \in \mathbb{R}^2$. In the sequel we focus on the behavior of the closed-loop trajectories on either side of the surface S_{ij}.

Denote $\boldsymbol{r}^-$, $\boldsymbol{r}^+$ the system (position) trajectories on either side of the switching surface S_{ij} (i.e., before and after crossing the switching surface). After some algebraic calculations one has:

$$\nabla S_{ij} \boldsymbol{f}(\boldsymbol{r}^-) = 2u_i^- ({\boldsymbol{r}_{ij}}^T \mathbf{F}_{gi})^- - 2u_j^- ({\boldsymbol{r}_{ij}}^T \mathbf{F}_{gj})^-, \quad (29a)$$

$$\nabla S_{ij} \boldsymbol{f}(\boldsymbol{r}^+) = 2(1 - \sigma_{ij}) \left(u_i^+ ({\boldsymbol{r}_{ij}}^T \mathbf{F}_{gi})^+ - u_j^+ ({\boldsymbol{r}_{ij}}^T \mathbf{F}_{gj})^+ \right) + 2\sigma_{ij} \left(u_i^+ ({\boldsymbol{r}_{ij}}^T \mathbf{F}_{oj}^i)^+ - u_j^+ ({\boldsymbol{r}_{ij}}^T \mathbf{F}_{oi}^j)^+ \right), \quad (29b)$$

where u_i^-, u_j^-, u_i^+, u_j^+ are the agents' linear velocities on either side of the surface S_{ij}, and the inner products in (29) are evaluated before and after crossing S_{ij}. The set of Zeno points is:

$$Z_{S_{ij}} = \{\boldsymbol{r} \in \mathbb{R}^{2N} \mid \dot{S}_{ij}(\boldsymbol{r}^-) = \dot{S}_{ij}(\boldsymbol{r}^+) = \ddot{S}_{ij}(\boldsymbol{r}^-) = \ddot{S}_{ij}(\boldsymbol{r}^+) = 0\}, \quad (30)$$

where $\dot{S}_{ij}$, $\ddot{S}_{ij}$ are the first and second derivatives of S_{ij} w.r.t. time along the system trajectories, and expresses the conditions under which the closed-loop system trajectories get stuck on S_{ij}. After some algebraic calculations, and taking into account that by construction: $u_i^- = u_i^+ = u_{i\epsilon}$, $u_j^- = u_j^+ = u_{j\epsilon}$, the first two of the Zeno conditions (30) read as in (31). We furthermore have:

$$({\boldsymbol{r}_{ij}}^T \mathbf{F}_{gi})^- = (\|\boldsymbol{r}_{ij}\|)^- \cos\psi_i^- = (d_c + \epsilon)\cos\psi_i^-, \quad (32a)$$

$$({\boldsymbol{r}_{ij}}^T \mathbf{F}_{gj})^- = (\|\boldsymbol{r}_{ij}\|)^- \cos\psi_j^- = (d_c + \epsilon)\cos\psi_j^-, \quad (32b)$$

$$({\boldsymbol{r}_{ij}}^T \mathbf{F}_{gi})^+ = (\|\boldsymbol{r}_{ij}\|)^+ \cos\psi_i^+ = (d_c - \epsilon)\cos\psi_i^+, \quad (32c)$$

$$({\boldsymbol{r}_{ij}}^T \mathbf{F}_{gj})^+ = (\|\boldsymbol{r}_{ij}\|)^+ \cos\psi_j^+ = (d_c - \epsilon)\cos\psi_j^+, \quad (32d)$$

$$({\boldsymbol{r}_{ij}}^T \mathbf{F}_{oj}^i)^+ = (\|\boldsymbol{r}_{ij}\|)^+ \cos 0 = (d_c - \epsilon), \quad (32e)$$

$$({\boldsymbol{r}_{ij}}^T \mathbf{F}_{oi}^j)^+ = (\|\boldsymbol{r}_{ij}\|)^+ \cos\pi = -(d_c - \epsilon), \quad (32f)$$

where ψ_i^-, ψ_i^+ are the angles of the vector field $\mathbf{F}_{gi}$ before and after the surface S_{ij}, respectively, and similarly, ψ_j^-, ψ_j^+ are the angles of the vector field $\mathbf{F}_{gj}$ before and after the surface S_{ij}. The system (31) is then further written as in (33). The system (33) is linear homogeneous; hence, if $\det(\Omega) \neq 0$, the unique solution is $u_{i\epsilon} = u_{j\epsilon} = 0$. In this case, $u_{i\epsilon} = 0 \Rightarrow u_{ic} = 0 \Rightarrow \|\boldsymbol{r}_i - \boldsymbol{r}_{gi}\| = 0 \Rightarrow \boldsymbol{r}_i = \boldsymbol{r}_{gi}$, and similarly for subscript j, that is, the agents i, j are already in their final destinations. If $\det(\Omega) = 0$ then the system (33) has infinitely many solutions, which implies that the Zeno conditions might be true for some non-zero values of $u_{i\epsilon}$, $u_{j\epsilon}$,

$$\begin{bmatrix} (\boldsymbol{r}_{ij}{}^T\mathbf{F}_{gi})^- & -(\boldsymbol{r}_{ij}{}^T\mathbf{F}_{gj})^- \\ \sigma_{ij}(\boldsymbol{r}_{ij}{}^T\mathbf{F}^i_{oj})^+ + (1-\sigma_{ij})(\boldsymbol{r}_{ij}{}^T\mathbf{F}_{gi})^+ & -\sigma_{ij}(\boldsymbol{r}_{ij}{}^T\mathbf{F}^j_{oi})^+ - (1-\sigma_{ij})(\boldsymbol{r}_{ij}{}^T\mathbf{F}_{gj})^+ \end{bmatrix} \begin{bmatrix} u_{i\epsilon} \\ u_{j\epsilon} \end{bmatrix} = \begin{bmatrix} 0 \\ 0 \end{bmatrix}. \tag{31}$$

$$\underbrace{\begin{bmatrix} (d_c+\epsilon)\cos\psi_i^- & -(d_c+\epsilon)\cos\psi_j^- \\ \sigma_{ij}(d_c-\epsilon)+(1-\sigma_{ij})(d_c-\epsilon)\cos\psi_i^+ & \sigma_{ij}(d_c-\epsilon)-(1-\sigma_{ij})(d_c-\epsilon)\cos\psi_j^+ \end{bmatrix}}_{\Omega} \begin{bmatrix} u_{i\epsilon} \\ u_{j\epsilon} \end{bmatrix} = \begin{bmatrix} 0 \\ 0 \end{bmatrix}. \tag{33}$$

that is, away from the goal destinations. We investigate this case. After some algebraic calculations: $\det(\Omega)=0 \Rightarrow$

$$\cos\psi_i^-(\sigma_{ij}-(1-\sigma_{ij})\cos\psi_j^+)+ \\ +\cos\psi_j^-(\sigma_{ij}+(1-\sigma_{ij})\cos\psi_i^+)=0. \tag{34}$$

If the condition (34) is true, then the solution of (33) is: $u_{i\epsilon}\cos\psi_i^- = u_{j\epsilon}\cos\psi_j^-$. This further reads that the Zeno conditions (31) hold true if the agents i, j get connected at locations $\boldsymbol{r}_i$, $\boldsymbol{r}_j$ at which the selected gains k_i, k_j, the goal locations $\boldsymbol{r}_{gi}$, $\boldsymbol{r}_{gj}$ and the angles ψ_i^-, ψ_j^- of the vector fields $\mathbf{F}_{gi}$, $\mathbf{F}_{gj}$ with the vector $\boldsymbol{r}_{ij}$ make the solution of (33) true. Since $u_{i\epsilon}, u_{j\epsilon} > 0$ and constant, it follows that $\frac{\cos\psi_i^-}{\cos\psi_j^-} > 0$ and constant. The second equation of (33) further reads:

$$\frac{\cos\psi_i^-}{\cos\psi_j^-} = -\frac{\sigma_{ij}+(1-\sigma_{ij})\cos\psi_i^+}{\sigma_{ij}-(1-\sigma_{ij})\cos\psi_j^+} = -\frac{\mu+\cos\psi_i^+}{\mu-\cos\psi_j^+} = \text{const},$$

where $\mu = \frac{\sigma_{ij}}{1-\sigma_{ij}}$. Denote $\Psi = -\frac{\mu+\cos\psi_i^+}{\mu-\cos\psi_j^+}$. For $\mu = 0$, that is, $\sigma_{ij} = 1$, one has: $\Psi_{\mu=0} = \frac{\cos\psi_i^+}{\cos\psi_j^+}$. Since $\Psi = \text{const}$, it follows that $\frac{\cos\psi_i^+}{\cos\psi_j^+} = \frac{\cos\psi_i^-}{\cos\psi_j^-} > 0$, and also that: $\frac{\partial\Psi}{\partial\mu} = 0 \Rightarrow \frac{\cos\psi_i^+ + \cos\psi_j^+}{(\mu-\cos\psi_j^+)^2} = 0 \Rightarrow \cos\psi_i^+ = -\cos\psi_j^+ \Rightarrow \frac{\cos\psi_i^+}{\cos\psi_j^+} = -1$, a contradiction. Hence there are no locations $\boldsymbol{r}_i$, $\boldsymbol{r}_j$, $\boldsymbol{r}_{gi}$, $\boldsymbol{r}_{gj}$ such that the Zeno conditions (31) hold true., i.e., $Z_{S_{ij}} = \emptyset$.

The case of T_{ij} can be treated similarly. Denote $\boldsymbol{r}^-$, $\boldsymbol{r}^+$ the system (position) trajectories on either side of the switching surface T_{ij}. After some algebraic calculations one has:

$$\nabla T_{ij}\boldsymbol{f}(\boldsymbol{r}^-) = 2(1-\sigma_{ij})\left(u_i^-(\boldsymbol{r}_{ij}{}^T\mathbf{F}_{gi})^- - u_j^-(\boldsymbol{r}_{ij}{}^T\mathbf{F}_{gj})^-\right) \\ +2\sigma_{ij}\left(u_i^-(\boldsymbol{r}_{ij}{}^T\mathbf{F}^i_{oj})^- - u_j^-(\boldsymbol{r}_{ij}{}^T\mathbf{F}^j_{oi})^-\right), \tag{35a}$$

$$\nabla T_{ij}\boldsymbol{f}(\boldsymbol{r}^+) = 2u_i^+(\boldsymbol{r}_{ij}{}^T\mathbf{F}^i_{oj})^+ - 2u_j^+(\boldsymbol{r}_{ij}{}^T\mathbf{F}^j_{oi})^+, \tag{35b}$$

where u_i^-, u_j^-, u_i^+, u_j^+ are the agents' linear velocities on either side of the surface T_{ij}, and the inner products in (35) are evaluated accordingly as:

$$(\boldsymbol{r}_{ij}{}^T\mathbf{F}_{gi})^- = (\|\boldsymbol{r}_{ij}\|)^-\cos\psi_i^- = (d_r+\epsilon)\cos\psi_i^-, \tag{36a}$$
$$(\boldsymbol{r}_{ij}{}^T\mathbf{F}_{gj})^- = (\|\boldsymbol{r}_{ij}\|)^-\cos\psi_j^- = (d_r+\epsilon)\cos\psi_j^-, \tag{36b}$$
$$(\boldsymbol{r}_{ij}{}^T\mathbf{F}^i_{oj})^- = (\|\boldsymbol{r}_{ij}\|)^-\cos 0 = (d_r+\epsilon), \tag{36c}$$
$$(\boldsymbol{r}_{ij}{}^T\mathbf{F}^j_{oi})^- = (\|\boldsymbol{r}_{ij}\|)^-\cos\pi = -(d_r+\epsilon), \tag{36d}$$
$$(\boldsymbol{r}_{ij}{}^T\mathbf{F}^i_{oj})^+ = (\|\boldsymbol{r}_{ij}\|)^+\cos 0 = (d_r-\epsilon), \tag{36e}$$
$$(\boldsymbol{r}_{ij}{}^T\mathbf{F}^j_{oi})^+ = (\|\boldsymbol{r}_{ij}\|)^+\cos\pi = -(d_r-\epsilon). \tag{36f}$$

The set of Zeno points is:

$$Z_{T_{ij}} = \{\boldsymbol{r}\in\mathbb{R}^{2N} \mid \\ \dot{T}_{ij}(\boldsymbol{r}^-) = \dot{T}_{ij}(\boldsymbol{r}^+) = \ddot{T}_{ij}(\boldsymbol{r}^-) = \ddot{T}_{ij}(\boldsymbol{r}^+) = 0\}, \tag{37}$$

and the first two conditions are written in matrix form as in (38). The determinant of the linear homogeneous system reads: $\det(\Omega) = \cos\psi_i^- + \cos\psi_j^-$. For $\det(\Omega)\neq 0$ the system (38) has only the trivial solution $u_{i\epsilon} = u_{j\epsilon} = 0$. For $\det(\Omega) = 0$ the system has infinitely many solutions. Let us also consider the third Zeno condition, which reads: $-u_{i\epsilon}(\sin\psi_i^-)\dot{\psi}_i^- + u_{j\epsilon}(\sin\psi_j^-)\dot{\psi}_j^- = 0$. This condition is true for $u_{i\epsilon}\neq 0$, $u_{j\epsilon}\neq 0$ (i.e., away from the goal locations $\boldsymbol{r}_{gi}$, $\boldsymbol{r}_{gj}$) and for any value of the agents' angular velocities (expressed via $\dot{\psi}_i^-$, $\dot{\psi}_j^-$), if $\sin\psi_i^- = \sin\psi_j^- = 0$. Therefore, the concurrent satisfaction of $\cos\psi_i^- + \cos\psi_j^- = 0$ and $\sin\psi_i^- = \sin\psi_j^- = 0$ yields either $\psi_i^- = 0$ and $\psi_j^- = \pi$, or $\psi_i^- = \pi$ and $\psi_j^- = 0$. These conditions reduce to the case when agents' positions $\boldsymbol{r}_i^-$, $\boldsymbol{r}_j^-$ and goal locations $\boldsymbol{r}_{gi}$, $\boldsymbol{r}_{gj}$ lie on the same line. The set of initial conditions from which agents' trajectories converge to the set $Z_{T_{ij}}$ is the set of initial positions $\boldsymbol{r}_i(0)$, $\boldsymbol{r}_j(0)$ lying on the line connecting the goal locations $\boldsymbol{r}_{gi}$, $\boldsymbol{r}_{gj}$, and of initial orientations $\theta_i(0)$, $\theta_j(0)$ coinciding with the orientation of the vector fields $\mathbf{F}^\star_i(\boldsymbol{r}_i(0))$, $\mathbf{F}^\star_j(\boldsymbol{r}_j(0))$. Hence the initial conditions are confined on $\mathbb{R}\times\{\arctan(\frac{\mathbf{F}^\star_{iy}(\boldsymbol{r}_i(0))}{\mathbf{F}^\star_{ix}(\boldsymbol{r}_i(0))}), \arctan(\frac{\mathbf{F}^\star_{jy}(\boldsymbol{r}_i(0))}{\mathbf{F}^\star_{jx}(\boldsymbol{r}_j(0))}\}$, i.e., on a lower dimensional manifold, and as thus is of measure zero. The case of $N>2$ agents can be treated accordingly. Consider an agent i lying at distance $d_{im} = d_c$ w.r.t. $M\leq(N-1)$ agents $m\neq i$. Define: $S_{im}(t) : \{\boldsymbol{r}_i(t), \boldsymbol{r}_m(t)\in\mathbb{R}^2 \mid \|\boldsymbol{r}_i(t) - \boldsymbol{r}_m(t)\| - d_c = 0\}$ the $M\leq(N-1)$ switching surfaces of agent i w.r.t. its neighbors m. This results in $\frac{NM}{2}$ switching surfaces, since for any pair of agents (i,m) it holds that: $S_{im} = S_{mi}$, and $(2NM)$ Zeno conditions. The concurrent satisfaction of all Zeno conditions reduces to the case when agents' positions and goal locations lie on the same line. Thus, the set of initial conditions from which the agents converge to Zeno positions are confined on a lower dimensional manifold, and as thus are of measure zero. This completes the proof. ■

Remark 9: Theorem 5 justifies that the set of initial conditions for which the multi-robot system exhibits Zeno trajectories, i.e., exhibits chattering across a switching surface for *infinite* amount of time (in other words, the set of initial conditions that result in deadlock for the multi-agent system with robots getting stuck away from their goal destinations) is of measure zero. To avoid the *finite-time* chattering that may result due to sliding along a switching surface, which is

$$\underbrace{\begin{bmatrix} \sigma_{ij}(d_r+\epsilon)+(1-\sigma_{ij})(d_r+\epsilon)\cos\psi_i^- & \sigma_{ij}(d_r+\epsilon)-(1-\sigma_{ij})(d_r+\epsilon)\cos\psi_j^- \\ (d_r-\epsilon) & (d_r-\epsilon) \end{bmatrix}}_{\Omega} \begin{bmatrix} u_{i\epsilon} \\ u_{j\epsilon} \end{bmatrix} = \begin{bmatrix} 0 \\ 0 \end{bmatrix}. \tag{38}$$

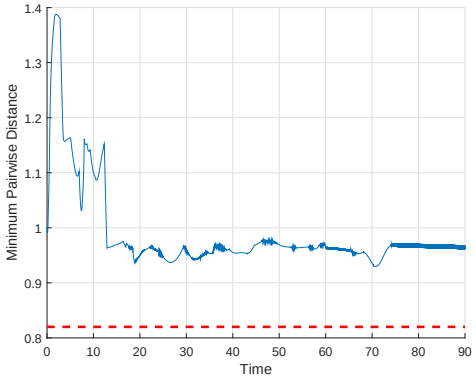

Fig. 8. Plot of the smallest pairwise distance d_{ij} among all pairs of agents (i,j) at each time instant t. The smallest pairwise distance remains always greater than the minimum separation 2ϱ.

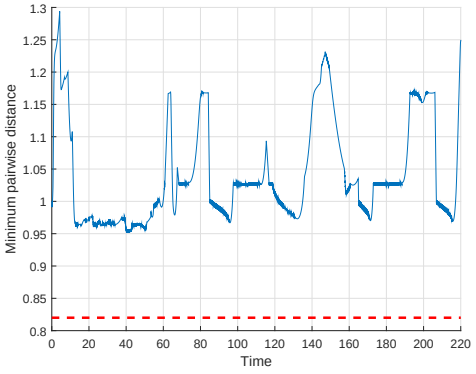

Fig. 10. Plot of the smallest pairwise distance d_{ij} among all pairs of class-A agents and all class-A - class-B pairs at each time instant t. The smallest pairwise distance remains always greater than the minimum separation 2ϱ.

undesired in practical applications, one can employ hysteresis logics [56].

C. Simulation Results

We consider two scenarios involving N = 20 agents which are assigned to move towards goal locations while avoiding collisions. Goal locations are selected to be sufficiently far apart so that the agents' communication regions do not overlap when agents lie on their goal locations. The radii of the agents are $\varrho = 0.4$, the minimum separation is set equal to $d_m = 2\varrho = 0.8$, and the communication radius is set equal to $R_c = 1.25$.

In the first scenario all agents are of class-A; hence they are always moving under (23a), (26). Their motion is depicted through the snapshots in Fig. 7. The smallest pairwise distance at each time instant is shown in Fig. 8, demonstrating that minimum separation is never violated.

In the second scenario, the agents start from the same initial conditions and head towards the same goal locations as with those in the first scenario, yet 4 out of 20 agents are of class-B. class-B agents move with upper bounded linear velocity, not necessarily with constant orientation, and they do not take into account any of the other agents. Hence, class-B agents model either agents of failed sensing/communication capabilities, or agents of higher priority which neglect and do not actively participate in ensuring safety. The motion of the agents is depicted in Fig. 9, with class-B agents illustrated in black color. class-B agents do not participate in collision avoidance, and thus they may collide into each other, as shown in Fig. 9(b). At simulation time $t = 100$ sec almost all class-A agents have safely converged to their goal locations, while class-B agents are moving with constant velocity towards class-A agents. Safety is ensured as the proposed control strategy forces class-A agents to move out of the way and avoid class-B agents. The evolution of the smallest pairwise distance among all pairs of class-A agents and between any class-A and any class-B agent is shown in Fig. 10, demonstrating that the minimum separation is never violated.

VI. Discussion and Conclusions

This paper presented a novel methodology on the motion planning of agents with unicycle kinematics in environments with circular obstacles, and its extension to the safe, semi-cooperative coordination for multiple agents belonging to different classes. The method is based on a family of vector fields whose integral curves exhibit attractive or repulsive behavior depending on the value of a parameter. It was shown that attractive-to-the-goal and repulsive-around-obstacles vector fields can be suitably blended in order to yield almost global feedback motion plans in environments with circular obstacles. In single-agent scenarios the method provides almost global feedback motion plans without requiring any parameter tuning in order to avoid local minima (or stable nodes), as other similar methods do. In multi-agent scenarios, the method builds upon the notion of semi-cooperative coordination, i.e., an ad-hoc prioritization among agents that facilitates conflict resolution and collision avoidance. Furthermore, it addresses agents belonging to different classes, such as agents of higher priority or failed sensing/communication systems or dynamic obstacles moving with upper bounded linear velocities.

One aspect that was not investigated formally in this paper is the effect of measurement noise and explicit external disturbances. Regarding external disturbances acting on the system dynamics, those that can be modeled as upper bounded velocities can be treated the same way as the case of moving obstacles; studying more sophisticated models of additive disturbances (e.g., wind effects) is left as an open problem. Regarding measurement noise, one conservative yet fairly

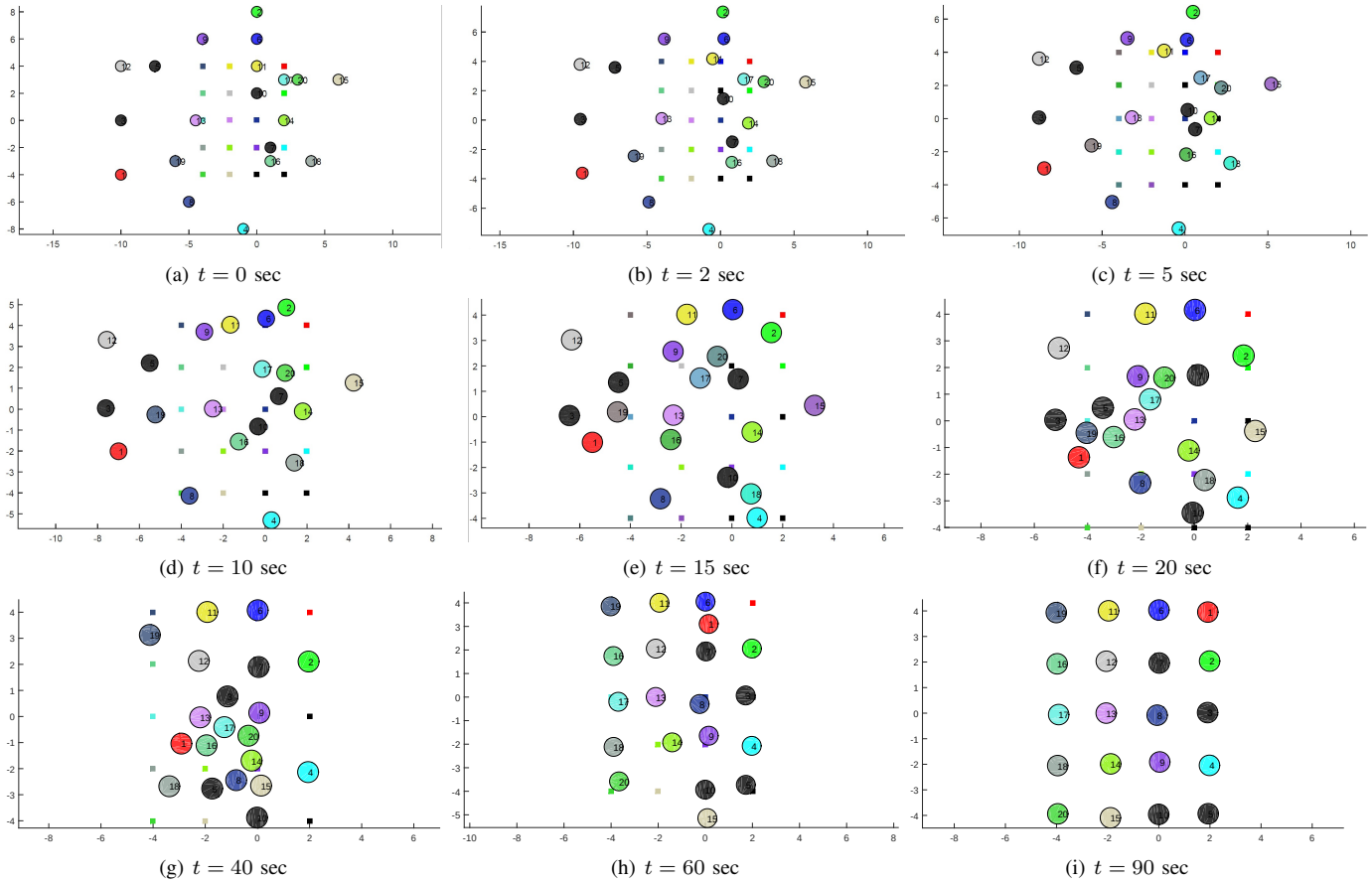

(a) $t = 0$ sec (b) $t = 2$ sec (c) $t = 5$ sec

(d) $t = 10$ sec (e) $t = 15$ sec (f) $t = 20$ sec

(g) $t = 40$ sec (h) $t = 60$ sec (i) $t = 90$ sec

Fig. 7. Collision-free motion of 20 agents under the proposed control strategy. All agents are of class-A.

straightforward approach would be to model the position and orientation errors as upper bounded disturbances with known bounds, and consider the design of the proposed protocol for the resulting perturbed multi-agent system. The conditions which couple the admissible noise with the vector fields and the control laws of the agents require a more extensive analysis, that is out of the scope and the limits of the current paper, and is left open as future work. In parallel, current work focuses on the definition of vector fields encoding input constraints, such as curvature bounds, which may be more appropriate for aircraft and car-like vehicles.

REFERENCES

[1] L. E. Parker, "Path planning and motion coordination in multiple mobile robot teams," in *Encyclopedia of Complexity and System Science*, R. A. Meyers, Ed. Springer, 2009.

[2] M. Kloetzer and C. Belta, "A fully automated framework for control of linear systems from temporal logic specifications," *IEEE Transactions on Automatic Control*, vol. 53, no. 1, pp. 287–297, Feb. 2008.

[3] H. Kress-Gazit, G. E. Fainekos, and G. J. Pappas, "Temporal-logic-based reactive mission and motion planning," *IEEE Transactions on Robotics*, vol. 25, no. 6, pp. 1370–1381, Dec. 2009.

[4] A. Bhatia, M. R. Maly, L. E. Kavraki, and M. Y. Vardi, "A multi-layered synergistic approach to motion planning with complex goals," *IEEE Robotics and Automation Magazine*, vol. 18, no. 3, pp. 55–64, 2011.

[5] R. Tedrake, I. R. Manchester, M. M. Tobenkin, and J. W. Roberts, "Feedback motion planning via sums-of-squares verification," *International Journal on Robotics Research*, vol. 29, no. 8, pp. 1038–1052, 2010.

[6] S. Karaman and E. Frazzoli, "Sampling-based algorithms for optimal motion planning," *International Journal on Robotics Research*, vol. 30, no. 7, pp. 846–894, 2011.

[7] W. Ren and Y. Cao, "Overview of recent research in distributed multi-agent coordination," in *Distributed Coordination of Multi-agent Networks*, ser. Communications and Control Engineering. Springer-Verlag, 2011, ch. 2, pp. 23–41.

[8] M. Mesbahi and M. Egerstedt, *Graph Theoretic Methods in Multiagent Networks*. Princeton University Press, 2010.

[9] W. Ren, R. W. Beard, and E. M. Atkins, "Information consensus in multi-vehicle cooperative control," *IEEE Control Systems Magazine*, vol. 27, no. 2, pp. 71–82, apr 2007.

[10] R. Olfati-Saber, J. A. Fax, and R. M. Murray, "Consensus and cooperation in networked multi-agent systems," *Proceedings of the IEEE*, vol. 97, no. 1, pp. 215–233, 2007.

[11] Q. Wang, H. Gao, F. Alsaadi, and T. Hayat, "An overview of consensus problems in constrained multi-agent coordination," *Systems Science and Control Engineering*, vol. 2, pp. 275–284, 2014.

[12] X. Wang, X. Li, Y. Cong, Z. Zeng, and Z. Zheng, "Multi-agent distributed coordination control: Developments and directions," *International Journal of Robust and Nonlinear Control*, 2015. [Online]. Available: http://arxiv.org/abs/1505.02595

[13] P. Lin, Y. Jia, and L. Li, "Distributed robust h_∞ consensus control in directed networks of agents with time-delay," *Systems & Control Letters*, vol. 57, pp. 643–653, 2008.

[14] J. Mei, W. Ren, and G. Ma, "Distributed containment control for lagrangian networks with parametric uncertainties under a directed graph," *Automatica*, vol. 48, pp. 653–659, 2012.

[15] Z. Qu, C. Li, and F. Lewis, "Cooperative control with distributed gain adaptation and connectivity estimation for directed networks," *International Journal of Robust and Nonlinear Control*, 2012.

[16] J. liang Zhang, D. lian Qi, and M. Yu, "A game theoretic approach for the distributed control of multi-agent systems under directed and time-varying topology," *International Journal of Control, Automation, and Systems*, vol. 12, no. 4, pp. 749–758, 2014.

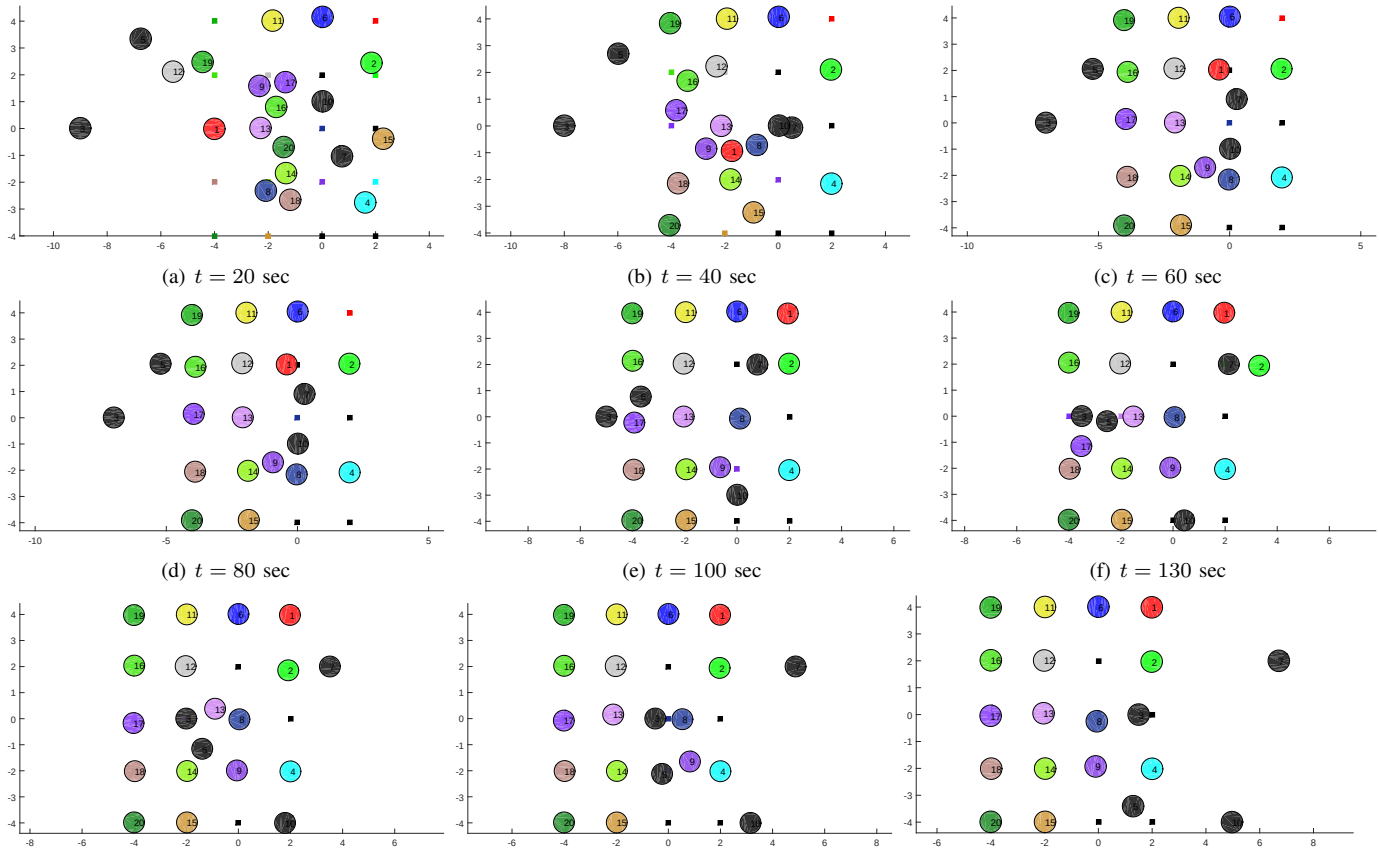

(a) $t = 20$ sec (b) $t = 40$ sec (c) $t = 60$ sec

(d) $t = 80$ sec (e) $t = 100$ sec (f) $t = 130$ sec

(g) $t = 160$ sec (h) $t = 190$ sec (i) $t = 230$ sec

Fig. 9. Collision-free motion of 20 agents under the proposed control strategy. 4 out of 20 agents (in black color) are of class-B.

[17] Z. Li, G. Wen, Z. Duan, and W. Ren, "Designing fully distributed consensus protocols for linear multi-agent systems with directed graphs," *IEEE Transactions on Automatic Control*, vol. 60, no. 4, pp. 1152–1157, Apr. 2015.

[18] Z. Li, X. Liu, and M. Fu, "Global consensus control of lipschitz nonlinear multi-agent systems," in *Proc. of the 18th IFAC World Congress*, Milano, Italy, Aug. 2011, pp. 10 056–10 061.

[19] M. Andreasson, D. V. Dimarogonas, and K. H. Johansson, "Undamped nonlinear consensus using integral lyapunov functions," in *Proc. of the 2012 American Control Conf.*, Montreal, Canada, Jun. 2012, pp. 6644–6649.

[20] K. Liu, G. Xie, W. Ren, and L. Wang, "Consensus for multi-agent systems with inherent nonlinear dynamics under directed topologies," *Systems & Control Letters*, vol. 62, no. 2, pp. 152–162, Feb. 2013.

[21] C. Li and Z. Qu, "Distributed finite-time consensus of nonlinear systems under switching topologies," *Automatica*, vol. 50, pp. 1626–1631, 2014.

[22] Z. Ding, "Consensus control of a class of lipschitz nonlinear systems," *International Journal of Control*, 2014.

[23] D. Panagou, D. M. Stipanović, and P. G. Voulgaris, "Distributed coordination and control of multi-robot networks using Lyapunov-like barrier functions," *Frontiers in Robotics and AI: Multi-Robot Systems*, p. doi: 10.3389/frobt.2015.00003, Mar. 2015.

[24] D. Panagou, M. Turpin, and V. Kumar, "Decentralized goal assignment and trajectory generation in multi-robot networks: A multiple lyapunov functions approach," in *Proc. of the 2014 IEEE Int. Conf. on Robotics and Automation*, Hong Kong, China, Jun. 2014, pp. 6757–6762.

[25] D. Panagou, D. M. Stipanović, and P. G. Voulgaris, "Distributed coordination and control of multi-robot networks using Lyapunov-like barrier functions," *IEEE Transactions on Automatic Control*, vol. 61, no. 3, pp. 617–632, 2016.

[26] D. Panagou and K. J. Kyriakopoulos, "Viability control for a class of underactuated systems," *Automatica*, vol. 49, no. 1, pp. 17–29, Jan. 2013.

[27] D. Panagou, H. G. Tanner, and K. J. Kyriakopoulos, "Control of nonholonomic systems using reference vector fields," in *Proc. of the 50th IEEE Conf. on Decision and Control and European Control Conf.*, Orlando, FL, Dec. 2011, pp. 2831–2836.

[28] D. Panagou, H. Tanner, and K. J. Kyriakopoulos, "Control design for a class of nonholonomic systems via reference vector fields and output regulation," *ASME Journal on Dynamic Systems, Measurement and Control*, Aug. 2015.

[29] G. Leitmann and J. Skowronski, "Avoidance control," *Journal of Optimization Theory and Applications*, vol. 23, pp. 581–591, Dec. 1977.

[30] O. Khatib, "Real-time obstacle avoidance for manipulators and mobile robots," *The International Journal of Robotic Research*, vol. 5, no. 1, pp. 90–98, Spring, 1986.

[31] E. G. Hernandez-Martinez and E. Aranda-Bricaire, "Convergence and collision avoidance in formation control: A survey of the artificial potential functions approach," in *Multi-Agent Systems - Modeling, Control, Programming, Simulations and Applications*, F. Alkhateeb, E. A. Maghayreh, and I. A. Doush, Eds. InTech, 2011, ch. 6, pp. 103–126.

[32] E. Rimon and D. Koditschek, "Exact robot navigation using artificial potential functions," *IEEE Transactions on Robotics and Automation*, vol. 8, no. 5, pp. 501–518, Oct. 1992.

[33] D. V. Dimarogonas and K. J. Kyriakopoulos, "Connectedness preserving distributed swarm aggregation for multiple kinematic robots," *IEEE Transactions on Robotics*, vol. 24, no. 5, pp. 1213–1223, Oct. 2008.

[34] S. G. Loizou and K. J. Kyriakopoulos, "Navigation of multiple kinematically constrained robots," *IEEE Transactions on Robotics*, vol. 24, no. 1, pp. 221–231, Feb. 2008.

[35] C. I. Connolly, J. B. Burns, and R. Weiss, "Path planning using Laplace's equation," in *Proc. of the 1990 IEEE Int. Conf. on Robotics and Automation*, May 1990, pp. 2102–2106.

[36] P. Szulczyński, D. Pazderski, and K. Kozłowski, "Real-time obstacle avoidance using harmonic potential functions," *Journal of Automation, Mobile Robotics and Intelligent Systems*, vol. 5, no. 3, pp. 59–66, 2011.

[37] S. Waydo and R. M. Murray, "Vehicle motion planning using stream functions," in *Proc. of the 2003 IEEE Int. Conf. on Robotics and Automation*, Taipei, Taiwan, Sep., pp. 2484–2491.

[38] A. D. Luca and G. Oriolo, "Local incremental planning for nonholo-

nomic mobile robots," in *Proc. of the 1994 IEEE Int. Conf. on Robotics and Automation*, May 1994, pp. 104–110.
[39] D. M. Stipanović, C. J. Tomlin, and G. Leitmann, "Monotone approximations of minimum and maximum functions and multi-objective problems," *Applied Mathematics and Optimization*, vol. 66, pp. 455–473, 2012.
[40] S. R. Lindemann and S. M. LaValle, "Simple and efficient algorithms for computing smooth, collision-free feedback laws over given cell decompositions," *The International Journal of Robotics Research*, vol. 28, no. 5, pp. 600–621, 2009.
[41] W. Dixon, T. Galluzo, G. Hu, and C. Crane, "Adaptive velocity field control of a wheeled mobile robot," in *Proc. of Fifth Int. Workshop on Robot Motion and Control*, Jun. 2005, pp. 145–150.
[42] T. Liddy, T.-F. Lu, P. Lozo, and D. Harvey, "Obstacle avoidance using complex vector fields," in *Proc. of the 2008 Australasian Conference on Robotics and Automation*, Canberra, Australia, Dec. 2008.
[43] E. G. Hernández-Martínez and E. Aranda-Bricaire, "Multi-agent formation control with collision avoidance based on discontinuous vector fields," in *Proc. of the 35th Annual Conf. of IEEE Industrial Electronics*, Nov. 2009, pp. 2283 –2288.
[44] D. Panagou, D. M. Stipanović, and P. G. Voulgaris, "Multi-objective control for multi-agent systems using Lyapunov-like barrier functions," in *Proc. of the 52nd IEEE Conference on Decision and Control*, Florence, Italy, Dec. 2013, pp. 1478–1483.
[45] R. Hegde and D. Panagou, "Multi-agent motion planning and coordination in polygonal environments using vector fields and model predictive control," in *Proc. of the European Control Conference*, Aalborg, Denmark, 2016.
[46] F. Blanchini and S. Miani, *Set-Theoretic Methods in Control*. Birkhauser, 2008.
[47] D. Panagou and V. Kumar, "Cooperative visibility maintenance for leader-follower formations in obstacle environments," *IEEE Transactions on Robotics*, vol. 30, no. 4, pp. 831–844, Aug. 2014.
[48] D. Panagou, "Motion planning and collision avoidance using navigation vector fields," in *Proc. of the 2014 IEEE International Conference on Robotics and Automation*, Hong Kong, China, Jun. 2014, pp. 2513–2518.
[49] ——, "Distributed coordination protocols for aggregation and navigation in multi-agent systems under local directed interactions," in *Proc. of the 54th IEEE Conference on Decision and Control*, Osaka, Japan, Dec. 2015, pp. 2780–2785.
[50] W. M. Boothby, *An Introduction to Differentiable Manifolds and Riemannian Geometry - 2nd Edition*. Academic Press, 1986.
[51] M. Henle, *A Combinatorial Introduction to Topology*. Dover Publications, 1994.
[52] J. M. Lee, *Introduction to Smooth Manifolds*. Springer, 2002.
[53] X. Tricoche, G. Scheuermann, and H. Hagen, "A topology simplification method for 2D vector fields," in *Proc. of Visualization 2000*, Salt Lake City, UT, USA, Oct., pp. 359–366.
[54] A. D. Ames and S. Sastry, "Characterization of Zeno behavior in hybrid systems using homological methods," in *Proc. of the 2005 American Control Conf.*, Portland, OR, USA, Jun. 2005, pp. 1160–1165.
[55] F. Ceragioli, "Finite valued feedback laws and piecewise classical solutions," *Nonlinear Analysis*, vol. 65, no. 5, pp. 984–998, 2006.
[56] D. Liberzon, *Switching in Systems and Control*. Birkhauser Boston, 2003.

APPENDIX A
PROOF OF THEOREM 2

Proof: Consider two points A, B of equal distance and on opposites sides w.r.t. the line l (Fig. 11). Their position vectors $\boldsymbol{r}_A = [x_A \;\; y_A]^T$, $\boldsymbol{r}_B = [x_B \;\; y_B]^T$ w.r.t. $\mathcal{G}$ read:

$$x_A = R\cos a, \qquad y_A = R\sin a, \tag{38a}$$
$$x_B = R\cos(2\varphi - a), \qquad y_B = R\sin(2\varphi - a), \tag{38b}$$

where (R, a), $(R, (2\varphi - a))$ are the polar coordinates of A, B, respectively. We need to prove that the vector $\mathbf{F}(\boldsymbol{r}_A)$, denoted $\mathbf{F}_A$, reflects to the vector $\mathbf{F}(\boldsymbol{r}_B)$, denoted $\mathbf{F}_B$, w.r.t. the line $l : y = \tan\varphi\, x$. The reflection matrix about the considered line l is: $\boldsymbol{H}(2\varphi) = \begin{bmatrix} \cos 2\varphi & \sin 2\varphi \\ \sin 2\varphi & -\cos 2\varphi \end{bmatrix}$. Substituting (38a)

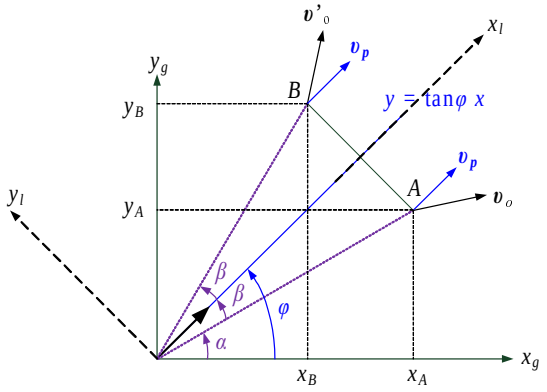

Fig. 11. The line $l : y = \tan\varphi\, x$, where $\varphi = \arctan(\frac{p_y}{p_x})$, is a reflection (or mirror) line for the vector field $\mathbf{F}$.

into (4) and after some algebraic calculations we get:

$$\mathbf{F}_A = \underbrace{\frac{(\lambda-2)R^2\|\boldsymbol{p}\|}{2}\begin{bmatrix}\cos\varphi \\ \sin\varphi\end{bmatrix}}_{\boldsymbol{v}_p} + \underbrace{\frac{\lambda R^2\|\boldsymbol{p}\|}{2}\begin{bmatrix}\cos(\varphi-2a) \\ -\sin(\varphi-2a)\end{bmatrix}}_{\boldsymbol{v}_o}, \tag{39}$$

where $\|\boldsymbol{p}\| = \sqrt{{p_x}^2 + {p_y}^2}$. Substituting (38b) into (4) yields:

$$\mathbf{F}_B = \underbrace{\frac{(\lambda-2)R^2\|\boldsymbol{p}\|}{2}\begin{bmatrix}\cos\varphi \\ \sin\varphi\end{bmatrix}}_{\boldsymbol{v}_p} + \underbrace{\frac{\lambda R^2\|\boldsymbol{p}\|}{2}\begin{bmatrix}\cos 2\varphi & \sin 2\varphi \\ \sin 2\varphi & -\cos 2\varphi\end{bmatrix}\begin{bmatrix}\cos(\varphi-2a) \\ -\sin(\varphi-2a)\end{bmatrix}}_{\boldsymbol{v}'_o}. \tag{40}$$

One has: $\mathbf{F}_A = \boldsymbol{v}_p + \boldsymbol{v}_o$ and $\mathbf{F}_B = \boldsymbol{v}_p + \boldsymbol{v}'_o$. Out of (39), (40) one gets that $\boldsymbol{v}'_o = \boldsymbol{H}(2\varphi)\boldsymbol{v}_o$, i.e., $\boldsymbol{v}'_o$ is the reflection of the vector $\boldsymbol{v}_o$ about the line l. Thus, one may write $\boldsymbol{v}_o = v^l_{ox}\hat{\boldsymbol{x}}_l + v^l_{oy}\hat{\boldsymbol{y}}_l$ and $\boldsymbol{v}'_o = v^l_{ox}\hat{\boldsymbol{x}}_l - v^l_{oy}\hat{\boldsymbol{y}}_l$, where $\hat{\boldsymbol{x}}_l$, $\hat{\boldsymbol{y}}_l$ are the unit vectors along the axes x_l, y_l, respectively, see Fig. 11. Furthermore, $\boldsymbol{v}_p$ is parallel to the vector $\boldsymbol{p}$, i.e., parallel to the candidate reflection line l. Consequently, one may write: $\boldsymbol{v}_p = v^l_{px}\hat{\boldsymbol{x}}_l + 0\;\hat{\boldsymbol{y}}_l$. It follows that: $\mathbf{F}_A = (v^l_{ox} + v^l_{px})\hat{\boldsymbol{x}}_l + v^l_{oy}\hat{\boldsymbol{y}}_l$, $\mathbf{F}_B = (v^l_{ox} + v^l_{px})\hat{\boldsymbol{x}}_l - v^l_{oy}\hat{\boldsymbol{y}}_l$, i.e., that the vector $\mathbf{F}_B$ is a reflection of vector $\mathbf{F}_A$ about the line l. This completes the proof. ■

APPENDIX B
PROOF OF THEOREM 3

Proof: Consider the polar coordinates $(r\cos\phi, r\sin\phi)$ of a point (x, y) where:

$$r = \sqrt{x^2 + y^2}, \quad \cos\phi = \frac{x}{r}, \quad \sin\phi = \frac{y}{r}. \tag{41}$$

After substituting (41) and $p_x = 1$, $p_y = 0$ into (4) the vector field components read:

$$\mathrm{F}_x = r^2\left((\lambda-1)\cos^2\phi - \sin^2\phi\right), \tag{42a}$$
$$\mathrm{F}_y = r^2\left(\lambda\cos\phi\sin\phi\right). \tag{42b}$$

An integral curve of (1) is by definition the solution of the system of ordinary differential equations:

$$\begin{matrix}\frac{dx}{dt} = \mathrm{F}_x \\ \frac{dy}{dt} = \mathrm{F}_y\end{matrix}, \quad \text{which further reads:} \quad \frac{dx}{dy} = \frac{\mathrm{F}_x}{\mathrm{F}_y}, \tag{43}$$

while the differentials between Cartesian and polar coordinates satisfy the formula:

$$\begin{bmatrix} dr \\ rd\phi \end{bmatrix} = \begin{bmatrix} \cos\phi & \sin\phi \\ -\sin\phi & \cos\phi \end{bmatrix} \begin{bmatrix} dx \\ dy \end{bmatrix}. \tag{44}$$

Plugging (44), (42) into (43) results in: $\frac{1}{r}\, dr = (\lambda{-}1)\frac{\cos\phi}{\sin\phi}\, d\phi$, while integrating by parts yields: $\ln(r) = (\lambda-1)\ln(\sin\phi) + \ln(c) \Rightarrow \ln(r) = \ln\left(c\, \sin^{(\lambda-1)}\phi\right) \Rightarrow r = c\, \sin^{(\lambda-1)}\phi \Rightarrow r = c\, \frac{y^{(\lambda-1)}}{r^{(\lambda-1)}} \Rightarrow r^{\lambda} = c\, y^{(\lambda-1)} \Rightarrow (x^2+y^2)^{\frac{\lambda}{2}} = c\, y^{(\lambda-1)}$, where $c \in \mathbb{R}$. This completes the proof. ■

APPENDIX C
PROOF OF LEMMA 1

Proof: The first two arguments have been proved in the previous section. To verify the third argument, consider the norm of vector field $\mathbf{F}_i$ in the blending region $\mathcal{D}_i : \{\boldsymbol{r} \in \mathbb{R}^2 \mid \varrho_{\mathcal{Z}i} < \|\boldsymbol{r} - \boldsymbol{r}_{oi}\| < \varrho_{\mathcal{F}i}\}$, which reads:

$$\|\mathbf{F}_i\| = \sqrt{1 - 2\sigma_i(1-\sigma_i) + 2\sigma_i(1-\sigma_i)\cos\alpha},$$

where α the angle between the vectors $\mathbf{F}_g^n$, $\mathbf{F}_{oi}^n$ at some point $\boldsymbol{r} \in \mathcal{D}_i$. Then, for $\boldsymbol{r} \notin \mathcal{V}_i$ one has that $\|\mathbf{F}_i\|$ vanishes at the points where σ_i is the solution of: $2(1-\cos\alpha){\sigma_i}^2 - 2(1-\cos\alpha)\sigma_i + 1 = 0$. The discriminant reads $\Delta = -4(1-\cos\alpha)^2$, which implies that there are no real solutions, i.e., that the vector field $\mathbf{F}_i$ is nonsingular for $\boldsymbol{r} \notin \mathcal{V}_i$. Moreover, for $\boldsymbol{r} \in \mathcal{V}_i$ one has $\mathbf{F}_{oi}^n = \mathbf{0}$, and therefore: $\|\mathbf{F}_i\| = \sigma_i \neq 0$.

Finally, to verify the fourth argument, consider first that the integral curves which do not intersect with the blending region $\mathcal{D}_i$ are convergent by construction to $\boldsymbol{r}_g$. Consider now the boundary $S_i : \{\boldsymbol{r} \in \mathbb{R}^2 \mid \|\boldsymbol{r} - \boldsymbol{r}_{oi}\|^2 - {\varrho_{\mathcal{F}i}}^2 = 0\}$ of the region $\mathcal{D}_i$ and let us analyze the behavior of the integral curves on the manifolds: $S_i^- : \{\boldsymbol{r} \in \mathbb{R}^2 \mid \|\boldsymbol{r} - \boldsymbol{r}_{oi}\| = \varrho_{\mathcal{F}i} + \delta\varrho\}$, $S_i^+ : \{\boldsymbol{r} \in \mathbb{R}^2 \mid \|\boldsymbol{r} - \boldsymbol{r}_{oi}\| = \varrho_{\mathcal{F}i} - \delta\varrho\}$, with $\delta\varrho > 0$ arbitrarily small. After some calculations:

$$\nabla S_i\ \mathbf{F}_i = 2(\boldsymbol{r} - \boldsymbol{r}_{oi})^T \mathbf{F}_g^n, \quad \nabla S_i^-\ \mathbf{F}_i = 2(\boldsymbol{r} - \boldsymbol{r}_{oi})^T \mathbf{F}_g^n.$$

For $\nabla S_i^+\ \mathbf{F}_i$, consider the following cases:

Case 1. The vector field $\mathbf{F}_{oi}^n$ satisfies: $(\boldsymbol{r} - \boldsymbol{r}_{oi})^T \mathbf{F}_{oi}^n = 0$, and therefore:

$$\nabla S_i^+\ \mathbf{F}_i = 2\sigma_i(\boldsymbol{r} - \boldsymbol{r}_{oi})^T \mathbf{F}_g^n.$$

Then: $(\nabla S_i^-\ \mathbf{F}_i)(\nabla S_i^+\ \mathbf{F}_i) > 0$, which implies that the integral curves cross the switching surface S_i and enter $\mathcal{A}_i$. Consider now the behavior of the integral curves in $\mathcal{A}_i$. Assume that $\nabla S_i^+\ \mathbf{F}_i = 2\sigma_i(\boldsymbol{r} - \boldsymbol{r}_{oi})^T \mathbf{F}_g^n > 0$; this would imply that $\nabla S_i\ \mathbf{F}_i > 0$ as well, i.e., that the integral curves did not cross S_i, a contradiction. Then: $\nabla S_i^+\ \mathbf{F}_i = 2\sigma_i(\boldsymbol{r} - \boldsymbol{r}_{oi})^T \mathbf{F}_g^n < 0$, which yields that the integral curves approach the boundary $T_i : \{\boldsymbol{r} \in \mathbb{R}^2 \mid \|\boldsymbol{r} - \boldsymbol{r}_{oi}\|^2 - {\varrho_{\mathcal{Z}i}}^2 = 0\}$ of the blending region $\mathcal{D}_i$. Denote $T_i^- : \{\boldsymbol{r} \in \mathbb{R}^2 \mid \|\boldsymbol{r} - \boldsymbol{r}_{oi}\| = \varrho_{\mathcal{Z}i} + \delta\varrho\}$ and note that: $\nabla T_i^-\ \mathbf{F}_i = \nabla S_i^+\ \mathbf{F}_i < 0$, and that $\nabla T_i\ \mathbf{F}_i = 0$, since on T_i one has $\sigma_i = 0$. Then, $\mathbf{F}_i \neq \mathbf{0}$ is tangent to T_i, which means that the integral curves slide along T_i, until reaching region $\mathcal{B}_i$.

Remark 10: The integral curves are not defined on the (unique) point on T_i where $\mathbf{F}_i = \mathbf{0}$. This further implies that system trajectories which either start or reach this point get stuck away from the goal configuration.

Let us now consider the pattern of the integral curves in the vicinity of the singularity and characterize the set of initial conditions from which the system trajectories end there. It was shown in the previous section that the integral curves around the singularity set $\mathcal{V}_i$ are departing the set, except for one integral curve which converges to $\mathcal{V}_i$. For this condition to occur *the goal orientation θ_g should be co-linear with the line the singularity set $\mathcal{V}_i$ lies on*. To see why, recall that the vector field in the blending region reads: $\mathbf{F}_i = \sigma_i \mathbf{F}_g^n$, and that the vector field $\mathbf{F}_g^n$ should point to the singularity set $\mathcal{V}_i$. Consequently, this condition arises if and only if the obstacle is positioned such that the direction of the vector $\boldsymbol{p}_i$ coincides with the direction of the vector $\boldsymbol{p}_g$. *Therefore, the set of initial conditions from which the integral curves of $\mathbf{F}_i$ converge to the singularity set $\mathcal{V}_i$ is of Lebesgue measure zero.* Note also that if the direction of $\boldsymbol{p}_g$ does not coincide with the direction of $\boldsymbol{p}_i$, then the singular points of $\mathbf{F}_i$ are confined in $\mathcal{Z}_i$ on a line segment of length ϱ_ε, correspond to the initial conditions from which solutions are not defined, and are reached by no integral curve.

Case 2. In region $\mathcal{B}_i$ one may follow a similar analysis to conclude that the integral curves exit $\mathcal{B}_i$.

In summary, the vector field (15) is safe and globally convergent almost everywhere, i.e., except for a set of initial conditions of measure zero. ■

Dr. Dimitra Panagou received the Diploma and PhD degrees in Mechanical Engineering from the National Technical University of Athens, Greece, in 2006 and 2012, respectively. Since September 2014 she has been an Assistant Professor with the Department of Aerospace Engineering, University of Michigan. Prior to joining the University of Michigan, Dr. Panagou was a postdoctoral research associate with the Coordinated Science Laboratory, University of Illinois, Urbana-Champaign (2012-2014), a visiting research scholar with the GRASP Lab, University of Pennsylvania (June 2013, fall 2010) and a visiting research scholar with the University of Delaware, Mechanical Engineering Department (spring 2009). Her research interests include the fields of planning, coordination and distributed control of complex systems, with applications in unmanned aerial systems, robotic networks and autonomous multi-vehicle systems (ground, marine, aerial, space). She is a member of the IEEE and the AIAA.